Am J Cancer Res 2016;6(6):1231-1252
www.ajcr.us /ISSN:2156-6976/ajcr0027826

Original Article

ATP13A3 and caveolin-1 as potential biomarkers for difluoromethylornithine-based therapies in pancreatic cancers

Meenu Madan[1], Arjun Patel[1], Kristen Skruber[1], Dirk Geerts[2], Deborah A Altomare[3], Otto Phanstiel IV[1]

[1]University of Central Florida College of Medicine, Department of Medical Education, 12722 Research Parkway, Orlando, Florida 32826, USA; [2]Erasmus University Medical Center, Department of Pediatric Oncology, Dr. Molewaterplein 50, 3015 GE Rotterdam, The Netherlands; [3]University of Central Florida, Burnett School for Biomedical Sciences, 6900 Lake Nona Blvd., Orlando, FL 32827, USA

Received March 9, 2016; Accepted April 15, 2016; Epub June 1, 2016; Published June 15, 2016

Abstract: The purpose of this paper was to better understand the role of polyamine transport in pancreatic cancers. This paper identifies potential biomarkers for assessing the relative tumor commitment to polyamine biosynthesis or transport. Cell lines with low polyamine import activity and low ATP13A3 protein levels appear committed to polyamine biosynthesis and required high concentrations of the polyamine biosynthesis inhibitor, difluoromethylornithine (DFMO) to inhibit their growth (e.g., AsPC-1 and Capan 1). In contrast, cell lines with high polyamine import activity and high ATP13A3 protein expression (e.g., L3.6pl) demonstrated a commitment to polyamine transport and required lower DFMO concentrations to inhibit their growth. Pancreatic cancer cell lines which were most sensitive to DFMO also gave the highest EC_{50} values for the polyamine transport inhibitors (PTIs) tested indicating that more PTI was needed to inhibit the active polyamine transport systems of these cell lines. Most significant is that the combination therapy of DFMO+PTI was efficacious against both cell types with the PTI showing low efficacy in cell lines with low polyamine transport activity and high efficacy in cell lines with high polyamine transport activity. High ATP13A3 protein expression and moderate to low Cav-1 protein expression was shown to be predictive of tumors which effectively escape DFMO via polyamine import. In summary, this report demonstrates for the first time the role of ATP13A3 in polyamine transport and its use as a potential biomarker along with Cav-1 to select tumors most susceptible to DFMO. These findings may help stratify patients in the ongoing clinical trials with DFMO-based therapies and help predict tumor response.

Keywords: Difluoromethylornithine (DFMO), polyamines, pancreatic cancer, ATP13A3, polyamine transport

Introduction

The native polyamines, putrescine (Put), spermidine (Spd) and spermine (Spm) are key resources required by mammalian cells for growth and proliferation. These low molecular weight aliphatic amines play critical roles in chromatin remodeling, translation, eIF-5A biosynthesis, and transcription [1]. Polyamines exist primarily as polycations at physiological pH and interact strongly with biological polyanions such as RNA and DNA [2]. Unlike inorganic cations (e.g., Mg^{+2}) the native polyamines can be biosynthesized. In addition, they can be imported from the extracellular milieu. The connection between increased polyamine metabolic flux, neoplasia and tumor spread is well established [3-5].

Compounds that disrupt polyamine homeostasis have been shown to be clinically useful for both the chemoprevention and treatment of human cancers [6, 7]. Biomass generation is a critical requirement for rapidly-proliferating cancer cells and the altered metabolism of specific cancers make them especially sensitive to polyamine-targeting therapies [1, 8]. Polyamine metabolites are needed to replicate the cancer cell's contents. For example, Spd is required for the formation of the novel aminoacid hypusine, a critical residue in the formation of the required initiation factor eIF-5A [1]. In short, certain can-

cers seem to be 'addicted' to polyamines and rely on a combination of intracellular polyamine biosynthesis and import to maintain high levels of intracellular polyamines. The import process involves the polyamine transport system (PTS) which is used to scavenge polyamines from the extracellular milieu. This addiction to polyamine metabolites provides an opportunity to selectively target cancers via their upregulated PTS [9-11].

In principle, cancer cells exclusively committed to polyamine biosynthesis (Case A) could be targeted by α-difluoromethylornithine (DFMO), a compound which irreversibly inhibits ornithine decarboxylase (ODC), a key enzyme involved in the first step of polyamine biosynthesis. In practice, however, DFMO as a single therapy has been more challenging because DFMO-treated cancer cells often respond by upregulating polyamine import to circumvent DFMO's blockade of polyamine biosynthesis. Alternatively, cells exclusively committed to polyamine import via high utilization of the PTS (Case B) could be targeted by cytotoxic polyamine-based compounds [9-11], which selectively enter and kill cells via the PTS [10] or via polyamine transport inhibitors (PTIs) [12-14]. As most cancers are expected to lie along the continuum of these two extremes (Cases A and B), combinations of these agents (e.g., DFMO+PTI) are expected to show promise even in the treatment of cancers with high tumor heterogeneity [6, 15]. In addition, polyamine transport has been shown to be increased in hypoxic tumors [16], and the combination therapy of DFMO+PTI holds promise for the treatment of recalcitrant solid tumor types with aberrant hypoxia signaling such as pancreatic cancers [13, 14, 17-19].

The DFMO+PTI combination therapy may provide a 'catch-all' technology for cell populations with different commitment levels to polyamine biosynthesis and transport and this approach may be especially relevant in pancreatic cancers, where multiple cell populations with the ability to form tumors and self-renew have been identified [6, 15, 20]. Moreover, a recent report by Rao et al. demonstrating the critical roles that polyamines play in developing pancreatic cancers provides further impetus for this study [21]. Combination therapies involving DFMO+PTI are expected to be more efficacious than DFMO alone because they block an important cellular escape mechanism (i.e., polyamine import) and can thereby potentiate the in vivo effects of DFMO [13, 14]. This report describes our progress in identifying the role of ATP13A3 and caveolin-1 (Cav-1) as biomarkers which indicate which cell types will best respond to the DFMO+PTI combination therapy.

Materials and methods

Reagents

DFMO was kindly provided by Dr. Patrick Woster (MUSC). Aminoguanidine was acquired from Sigma-Aldrich (St. Louis, MO), spermidine (Spd) from Acros Organics (Geel, Belgium), and ^{3}H-Spd from Perkin-Elmer Inc, (Boston, MA). The primary rabbit polyclonal antibodies against ATP13A3 and caveolin-1 were purchased from Abgent (San Diego, CA) and from Santa Cruz Biotechnology (Dallas, TX), respectively. The primary rabbit monoclonal antibodies against c-Myc, MTAP, and p16 were purchased from Abcam (Cambridge, MA). The primary mouse monoclonal antibody against β-actin was obtained from Sigma-Aldrich. The secondary antibodies used included goat anti-rabbit and goat anti-mouse antibodies from Santa Cruz Biotechnology. All cell culture media and reagents were purchased from Life Technologies (Grand Island, NY). FBS was purchased from Atlanta Biologicals (Norcross, GA). All siRNA reagents, including ATP13A3 siRNA, scrambled siRNA and the Viromer Blue transfection agent were obtained from OriGene (Rockville, MD).

Cell culture

The L3.6pl pancreatic cell line was a gift from Dr. Isaiah Fidler at MD Anderson Cancer Center at Houston TX. hTERT-HPNE cells were a generous gift from Dr. Cheryl Baker at BioCurity Holdings, Inc. in Orlando, FL. CHO-K1 cells and CHO-MG cell lines were a gift from Dr. Wayne Flintoff at the University of Western Ontario, Canada. Other cell lines (AsPC-1, BxPC-3, Capan-1, MiaPaca-2, Pan02, Panc-1, and Su86.86) were purchased from ATCC (Manassas, VA), first cultured in the growth media suggested by ATCC and then shifted to RPMI 1640 media with 10% fetal bovine serum (FBS) and 1% penicillin/streptomycin, to allow testing of all cell lines under the same conditions. In the human cancer cell lines, 250 μM aminogua-

nidine was added to the media to prevent serum oxidase activity on polyamine-based compounds. For CHO and CHO-MG cells, 1 mM aminoguanidine was used. The media contained L-proline (2 μg/mL) for proper growth of the CHO-MG cells. Cells in early to mid-log phase were used for all experiments. All cells were grown at 37°C under a humidified 5% CO_2 atmosphere.

Cell treatments

Cells were grown to 70-80% confluence. The cells were then trypsinized and re-plated at the appropriate cell density depending on the length of drug treatment. Prior to drug addition, the cells were incubated for 24 h (to facilitate re-attachment) before adding the appropriate compound or vehicle in PBS. DFMO dosage was adapted according to the length of incubation and cell line while Spd was used at 1 μM for all experiments. The cells were incubated for either 48 h or 72 h depending upon the experiment, with aminoguanidine present in the media.

IC_{50} and IC_{10} determinations

Cell growth was assayed in sterile 96-well microtiter plates (Costar 3599, Corning, NY). CHO and CHO-MG cells were plated at 1000 cells/well. All the pancreatic cell lines were plated at 500 cells/well, except Su86.86 which was plated at 1500 cells/well and incubated overnight. As these experiments required three additives, cells were plated in 70 μL volumes. DFMO, Spd or polyamine drug solutions (10 μL/well) of appropriate concentration in phosphate-buffered saline (PBS) were added. When needed, additional PBS was added to ensure that each well had a total volume of 100 μL for the experiment. After incubation with the compound(s) for 72 h, cell growth was determined by measuring formazan formation from the 3-(4,5-dimethylthiazol-2-yl)-5-(3-carboxymethoxyphenyl)-2-(4-sulfenyl)-2H tetrazolium, inner salt (MTS) using a SynergyMxBiotek microplate reader for absorbance (490 nm) measurements. All experiments were performed in triplicate. IC_{50} and IC_{10} values (i.e., the concentration of the compound needed to maintain 50% and 90% viability, respectively), were calculated. Thus, the IC_{10} value defines the maximum concentration of the compound which a cell line can tolerate with minimal toxic effects to the cell (≤ 10% toxicity).

Rescue assay and EC_{50} determination

Cells were seeded in 96 well plates as above and were exposed to the respective IC_{50} DFMO dose for that cell line, with or without a rescuing amount of Spd (1 μM) for 72 h. This rescue from DFMO treatment with exogenous Spd was cell-line dependent. For example, in L3.6pl cells the 72 h DFMO IC_{50} value was 4.2 mM and gave 50% viability. Spd addition to these DFMO treated L3.6pl cells resulted in 90% viability and defined a window spanning from DFMO only (50%) to DFMO+Spd (90% viability). The EC_{50} was defined as the concentration of the PTI needed to traverse halfway between these two endpoints (in this case the [PTI] needed to achieve 70% viability in the presence of DFMO+Spd). This approach allows ranking of the PTIs in different cell lines since it considers the different response to a fixed concentration of Spd (1 μM) in each of the DFMO-treated cell lines.

siRNA treatment and ATP13A3 knockdown

Three siRNAs against ATP13A3 along with a scrambled siRNA were purchased from OriGene. The effect on ATP13A3 expression as measured by immunoblot are as follows: ATP13A3 siRNA #1 (Cat# SR312433A) - poor knockdown, ATP13A3 siRNA #2 (Cat# SR312433B) - maximal knockdown, ATP13A3 siRNA #3 (Cat# SR312433C) - moderate knockdown. ATP13A3 siRNA #2 demonstrated the best knockdown of all three siRNAs tested and was used for all subsequent experimentation. For the experiments, L3.6pl cells were grown to 70-80% confluence in the presence of either ATP13A3 siRNA #2 or scrambled siRNA complexed with the Viromer Blue transfection agent. After 48 h incubation with the appropriate siRNA/transfection agent complexes, cells were washed with PBS, harvested by trypsinization, and re-plated into sterile 96-well plates at 500 cells/well. As described above, the rescue assay (48 h) was performed on the siRNA-treated cells to determine rescue efficiency with and without ATP13A3 knockdown and used DFMO (8 mM), Spd (1 μM) and aminoguanidine (250 μM). ATP13A3 knockdown was confirmed by western blotting. Since the scrambled siRNA treated cells behaved like non-siRNA treated cells in terms of their Spd rescue profile, we concluded that the reduced viability observed with the ATP13A3 siRNA treated cells was not due to general siRNA cell stress but due to the specific reduction in ATP13A3 expression.

Table 1. Kinetic profiles (V_{max} and K_m) of human pancreatic cancer cell lines, murine (Pan02) and Chinese hamster ovary (CHO) cells

Cell line	V_{max} (^{3}H Spd) (nmoles/mg protein/min)	K_m for Spd (μM)
HPNE	1.8	0.19 ± .02
L3.6pl	24	0.67 ± .07
Panc-1	13	0.31 ± .01
Su86.86	7.0	0.29 ± .01
BxPC-3	9.0	0.18 ± .01
AsPC-1	2.3	0.12 ± .03
Capan-1	0.8	0.18 ± .02
Pan02	9.0	0.36 ± .05
CHO	3.0	0.24 ± .06
CHOMG	0	ND

Legend: Aminoguanidine (AG, 250 μM) was added to all pancreatic and HPNE cell lines and AG (at 1 mM) was added for CHO cell experiments to prevent amine oxidase activity present in the fetal bovine serum used for cell culture. These AG concentrations were non-toxic to the respective cell lines in separate experiments (not shown). The K_i values for the PTIs, trimer44 (**5a**), trimer44NMe (**5b**) and Lys-Spm (**6**) in L3.6pl human pancreatic cancer cells, were 36, 55, and 26 nM, respectively.

V_{max} determination

The kinetic profiles for Spd uptake and the ability of the PTIs to inhibit Spd uptake in the cell lines were determined using the protocols of Weeks et al. [19] Briefly, the respective cells (100,000/well) were seeded into a 24-well plate for log phase growth and incubated for 24 h at 37°C. The media was then replaced with preheated Hanks Balanced Salt Solution (HBSS, containing Ca^{+2} and Mg^{+2}) at 37°C. For K_m and V_{max} determinations ^{3}H-Spd was added at a range of 0-3 μM/well. For K_i determinations (**Table 1** footnote) ^{3}H-Spd (1 μM final concentration) was added with the respective PTI at different PTI concentrations (0, 0.1, 0.3, 1, 2 or 3 μM). Cells were incubated at 37°C for 15 min. The cells were then washed with cold HBSS and lysed with 0.1% sodium dodecyl sulfate (SDS) in water (500 μL). Each cell lysate was then transferred to an Eppendorf tube and centrifuged at 15,000 rpm for 15 min. A sample of each supernatant (200 μL) was transferred into a scintillation vial containing 2 mL of Scintiverse BD (Fisher Chemical, Pittsburgh, PA), and the resulting scintillation counts were measured. The amount of protein was determined using the Pierce BCA protein assay kit (Pierce, Rockford, IL) from the remaining lysate volume (approximately 300 μL) to normalize the radioactive counts obtained and the data reported as nmol ^{3}H-Spd/mg protein. K_i and K_m values were determined using double reciprocal Lineweaver-Burk plots. The K_i value was determined from the equation $K_i = IC_{50}/(1 + (L + K_m))$, where IC_{50} is the concentration of PTI required to block 50% of the relative uptake of ^{3}H-Spd and L is the concentration of ^{3}H-Spd used in the assay (1 μM). The K_m and V_{max} for Spd was calculated by plotting the inverse of [^{3}H-Spd] versus the inverse of the nmol Spd/mg protein/min. The K_m = −1/x intercept, and V_{max} = 1/Y intercept.

Western blot analysis

Cells were grown to 70-80% confluence, washed with cold PBS, and harvested in PBS after centrifugation. Cell lysates were prepared in standard RIPA buffer. Protein concentration was measured with the Pierce BCA Assay kit. For western blotting, equal quantities of protein (50-75 μg) were loaded onto SDS-PAGE gels. Protein was transferred to a nitrocellulose membrane (Bio-Rad, Hercules, CA) and blocked with 5% non-fat dry milk in PBS with 0.1% Tween-20 (PBS-T). Membranes were incubated with primary antibodies overnight at 4°C at respective dilutions [ATP13A3 (1:500), Cav-1 (1:500), c-Myc (1:1000), MTAP (1:1000), p16 (1:500), β-actin (1:25,000)]. The next morning, the membrane was washed with phosphate buffer saline containing 0.1% Tween-20 (PBS-T). The membrane was then incubated for 1 h at room temperature in the respective secondary antibodies (1:10,000) conjugated to horseradish peroxidase. Protein bands were visualized using the SuperSignal West Pico ECL kit (Pierce) and subsequent exposure to X-ray films. For re-probing, the membranes were stripped with Restore PLUS stripping buffer (Life Technologies) and re-probed with the β-actin antibody as a loading control. The intensity of the protein exposures on the X-ray film was evaluated by densitometry using ImageJ software (National Institutes of Health, Bethesda, MD). The data is presented as intensity of protein of interest divided by intensity of β-actin in each respective lane.

ATP13A3 and Cav-1 mRNA expression analysis in public human cancer datasets

Genome-wide mRNA expression profiles of 238 different datasets containing human cancer

samples were retrieved from the public Gene Expression Omnibus (GEO) dataset at the NCBI website http://www.ncbi.nlm.nih.gov/geo/ [22], from the EBI Express website http://www.ebi.ac.uk/arrayexpress/, and from the TCGA consortium website https://tcga-data.nci.nih.gov/tcga/, as annotated in Table S4. The data for the GSK-950 and Sadanandam-47 cell line sets used in Table S1 were from http://cbiit.nci.nih.gov and NCBI GEO (GSE17891), respectively. The large majority of studies were on the Affymetrix Gene Chip Human Genome U133A and Plus 2.0 platforms (U133A/U133P2; Affymetrix, Santa Clara, CA). CEL data were downloaded, and analyzed as described [23]. Briefly, gene transcript levels were determined from data image files using GeneChip operating software (MAS5.0 and GCOS1.0, from Affymetrix). Samples were scaled setting the average intensity of the middle 96% of all probe-set signals to a fixed value of 100 for every sample in the dataset, to allow transcript level comparison between samples and between studies. We determined significant present ("present call") and absent expression using this software. The TranscriptView genomic analysis and visualization tool (http://bioinfo.amc.uva.nl/human-genetics/transcriptview/) was used to select probe-sets, except Agilent G4502 array probes, for which no sequence data were available. Probes had to show unique mapping in an anti-sense position within (late) coding exons and/or the 3' UTR of the gene. When multiple correct probe-sets were available for a gene, the probe-set with the highest average expression and the highest amount of present calls for that dataset were used. The probe-sets selected for analysis of U133A/P2 arrays were 204069_at and 223282_at, for Illumina WG-6 v3.0 arrays 1663684 and 21-49226, and for Agilent HG 4x44K arrays 24_P183094 and 23_P134454, for ATP13A3 and Cav-1, respectively. Analyses were performed using R2; a genomics analysis and visualization platform developed in the Department of Oncogenomics, Academic Medical Center, Amsterdam, The Netherlands (http://r2.amc.nl). Website standard settings were used for all tests on Oncomine (http://www.oncomine.org).

Statistical analysis of public human cancer datasets

Correlations between ATP13A3 and Cav-1 mRNA expression (**Figures 8** and **9**, Table S4) were calculated using a Pearson test on 2log-transformed expression values (with the significance of a correlation determined by t = R/sqrt((1-r^2)/(n-2)), where R is the correlation value and n is the number of samples, and distribution measure is approximately as t with n-2 degrees of freedom). Significant correlations were only calculated for datasets when ≥ 10% of samples had a present call for both genes. The Statistical Package for the Social Sciences software package for Windows (Version 13.0) was used for all statistical analyses. Numerical results (Table S1) are expressed as the mean value ± SEM. When values are shown as 2log-median centered (**Figure 9A-D**, Tables S2 and S3), statistically significant differences were determined by t-testing. Results were considered significant when $p < 0.05$.

Results and discussion

Due to the broad context of this study, which incorporates the interplay between polyamine metabolism, oncogenes and transport activity, a brief overview is warranted.

Polyamine homeostasis via biosynthesis and transport

Polyamine homeostasis requires that polyamine biosynthesis and transport be intimately linked and balanced. The polyamine biosynthesis pathway is well understood [1] and relies on S-adenosylmethionine (SAM) and ornithine resources, which are derived from the aminoacids methionine and arginine, respectively. A detailed description is shown in **Figure 1**.

Intricate intracellular control mechanisms maintain polyamine levels via regulation of biosynthesis and transport. For example, antizyme 1 (AZ) is considered a dual regulator of polyamine biosynthesis and transport [1, 24, 25]. High intracellular polyamine levels cause a +1 translational frameshift which aligns two open reading frames and produces a full length AZ protein. AZ then binds to ornithine decarboxylase (ODC) to form an inactive ODC:AZ heterodimer and facilitates its degradation via the proteasome, thereby inhibiting polyamine biosynthesis [26, 27]. AZ induction also inhibits polyamine transport by an unknown mechanism [28-30]. In another example, inhibition of ODC with DFMO, results in a concomitant increase in polyamine import activity [13, 14, 31, 32] in an attempt to maintain cellular polyamine homeostasis. In summary, while there is evi-

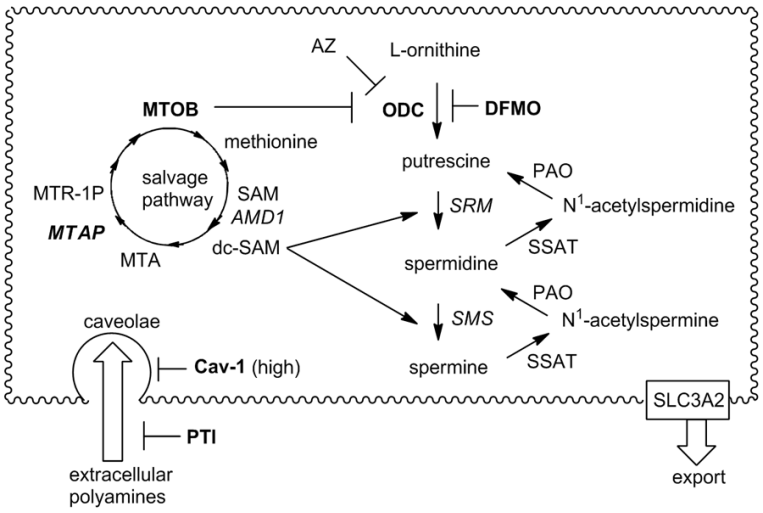

Figure 1. Human polyamine biosynthesis, metabolism and transport and the methionine salvage pathway. Ornithine decarboxylase (ODC) converts ornithine to putrescine and then spermidine synthase (SRM) appends an aminopropyl fragment derived from decarboxylated S-adenosylmethionine (dc-SAM) to putrescine to form Spd. The dc-SAM is generated by the action of adenosylmethionine decarboxylase (AMD1) on SAM. Spermine synthase (SMS) performs a similar task with dc-SAM to convert Spd to spermine (Spm). Catabolic enzymes like spermidine/spermine acetyl transferase (SSAT) and polyamine oxidase (PAO) allow for back-conversion from the higher polyamines (Spd and Spm) to putrescine (Put) as well as the formation of *N*-acetylated polyamines for cell export (presumably via SLC3A2 as seen in colon cancer cells). Abbreviations: *AMD1* (adenosylmethionine decarboxylase), AZ (antizyme), Cav-1 (caveolin-1), dc-SAM (decarboxy-S-adenosylmethionine), DFMO (difluoromethylornithine), MTA (5'-methylthioadenosine), MTAP (S-methyl-5'-thioadenosine phosphorylase), MTOB (methylthiooxobutyrate), MTR-1P (methylthioribulose phosphate), ODC (ornithine decarboxylase), PAO (polyamine oxidase), PTI (polyamine transport inhibitor), SAM (S-adenosyl-L-methionine), SLC3A2 (diamine exporter), SMS (spermine synthase), SRM (spermidine synthase), SSAT (spermidine/spermine acetyltransferase). Note: a direct back-conversion from Spm to Spd is possible via spermine oxidase (not shown).

dence linking polyamine biosynthesis and transport, the actual biomolecules involved in this connection are largely unknown.

Biomarkers of polyamine transport and oncogenes

A handful of candidate proteins involved in polyamine import have been reviewed [31], but no comprehensive molecular explanation of how they work in concert to maintain polyamine homeostasis is yet available. These important gaps in our knowledge preclude a full understanding of polyamine homeostasis and have delayed the identification of valid biomarkers for polyamine transport in human cancers. These biomarkers are needed to stratify cancer patients with tumors which will best respond to DFMO or which may require DFMO+PTI therapy.

While it is widely known that cancer cells have increased intracellular polyamine levels, it is less clear whether these levels are achieved through increased biosynthesis or a combination of biosynthetic and import processes. Polyamine transport biomarkers would help identify where along the continuum (between Case A and Case B) specific cancer types lie. As cross-talk exists between the synthetic route and the PTS (e.g., via AZ induction), cells can shift their sources of polyamines to avoid a particular pharmacologic intervention, e.g., DFMO. Biomarkers which track this shift over time could inform drug dosing and the effectiveness of combination therapies to address this escape response. A first step in identifying these biomarkers is to understand the relationships between key oncogenic signaling pathways and polyamine metabolism.

Oncogenes and polyamine transport

The interplay of oncogenes and polyamine metabolism has been recently reviewed [1]. The Ras signaling pathway was of interest for our study because K-Ras-activating oncogenic mutations causing uncontrolled cell growth are found in the vast majority (> 90%) of pancreatic ductal adenocarcinomas (PDACs) and there is a critical need to develop new interventions for this deadly form of cancer [33]. The canonical Ras signaling pathway involves the Raf, MEK1/2, Erk1/2 and c-Myc proteins, which play critical roles in cell growth and metabolism. However, the relationships between these oncogenic proteins and putative polyamine transport proteins, like caveolin-1 (Cav-1), in pancreatic cancers are poorly understood. Due to our limited understanding of polyamine transport, there are few reports detailing the connection between polyamine transport proteins and oncogenes.

In colorectal cancers, Cav-1 has been shown to be a negative regulator of polyamine import [34]. In addition, activated K-Ras was shown to decrease the expression of the putative putrescine export protein SLC3A2 in HCT116 colon cancer cells [35]. Therefore, at least in HCT116 cells, *activated K-Ras increases polyamine import and slows polyamine export*, leading to elevated intracellular polyamine levels. Together these results suggest that Cav-1 expression may provide insight into a tumor's dependence on polyamine import processes, where low Cav-1 expression is associated with high polyamine transport activity.

Bergeron and Porter first explored the effect of specific oncogene expression on polyamine metabolic enzymes and transport. Specifically, Rat-1 cells were stably transfected with Ras or N-myc oncogenes [36]. ODC activity was shown to be approximately 12-times higher in Ras-transfected cells, than in the parent or N-myc-transfected cell lines [36]. In contrast, polyamine transport was significantly increased in N-myc-transfected cells [36]. These authors concluded that the "associations between N-myc and Ras expression and critical aspects of polyamine metabolism suggest a possible role for the latter in facilitating the growth promoting properties of these oncogenes" [36].

The connection between the Myc family of proteins and polyamine transport activity is important because the Myc transcription factors affect polyamine biosynthesis by up-regulation of ODC transcription [1]. Specifically, Myc dimerizes with a partner protein, Max, and the Myc-Max complex binds to E-box motifs (CACGTG) in the ODC promoter activating ODC transcription [1]. ODC expression enhances putrescine biosynthesis and subsequent biosynthesis of the higher polyamines, Spd and Spm, via additional biosynthetic steps involving dc-SAM (**Figure 1**). ODC activity is sufficient for tumor promotion and ODC is considered a proto-oncogene [37]. As expected, cells which overexpress Myc have elevated levels of polyamines [1]. In this regard, Myc is key to increased intracellular polyamine levels because its up-regulation is known to increase polyamine biosynthesis and presumably import [36]. Lastly, a feedback mechanism has been proposed where the polyamines themselves regulate c-Myc translation through Chk2-dependent HuR phosphorylation [38]. Therefore, we surmised that Myc-driven tumors are likely 'addicted' to polyamines and may be especially sensitive to combination therapies which target polyamine biosynthesis and transport.

Since K-Ras mutations are prevalent in > 90% of PDACs and the Myc family genes are activated in nearly 70% of human cancers [1], we were interested in whether pancreatic cell lines with K-Ras mutations and high c-Myc expression also had high polyamine transport activity. We also investigated whether other genes associated with polyamine import in the literature (e.g., Cav-1), tracked with the polyamine import properties of pancreatic cancers (e.g., V_{max} of ^{3}H-Spd import).

To gain a better understanding of the relationships between specific protein expression and polyamine transport properties of pancreatic cancer cells, several human pancreatic cancer cell lines were characterized in terms of their sensitivity to DFMO, K_m and V_{max} values for ^{3}H-Spd import, and the ability of Spd to rescue the cells from a DFMO IC_{50} dose challenge. This data was then correlated with the relative expression patterns of proteins thought to play a role in polyamine transport. In addition, three known polyamine transport inhibitors (PTIs) [13, 14, 39] and DFMO were evaluated in the treatment of human pancreatic cancer cell lines in vitro to better understand how their relative protein expression patterns and basal V_{max} properties affected the efficacy of DFMO-only and DFMO+PTI therapies.

Cell line selection and biomarker rationale

Six human pancreatic cancer cell lines (AsPC-1, BxPC-3, Capan-1, L3.6pl, PanC-1, and Su-86.86) and one murine pancreatic cancer line (Pan02) were studied along with immortalized normal human pancreatic duct cells (HPNE) as a control. These cell lines were selected based upon their expected differential expression of key proteins (e.g., ATP13A3, Cav-1, c-Myc, MTAP, and p16). All human pancreatic cell lines tested here have known K-Ras mutations [40], except for BxPC-3 cells [41]. HPNE cells were used as a baseline control and represent intermediary cells formed during acinar to ductal metaplasia. Pan02 mouse pancreatic cancer cells were also evaluated to support future *in vivo* comparisons in immune-competent and immune-compromised mice [42]. Chinese hamster ovary cells with active (CHO-K1) and

deficient polyamine transport (CHO-MG) were used as additional controls.

The expression of each target protein was re-determined in this study for confirmation. MTAP is a key protein involved in recycling of methylthioadenosine (MTA, a byproduct of polyamine biosynthesis) to methionine (**Figure 1**) [43]. The pancreatic cell lines BxPC-3, CAPAN-1, PanC-1, and Su86.86 were confirmed to be MTAP-deficient, while AsPC-1 and L3.6pl were found to be MTAP positive. The V_{max} and K_m values for ^{3}H-Spd import and DFMO IC_{50} values were determined for each cell line (**Table 1**) along with the relative expression of putative polyamine transport proteins ATP13A3, Cav-1, c-Myc, and MTAP, as well as the tumor suppressor p16 protein in each cell line during logarithmic growth. These data then allowed for a better description of how relative protein expression patterns correlated to polyamine import processes.

The rationale for the selected protein markers was as follows:

MTAP and p16

The S-methyl-5'-thioadenosine phosphorylase (MTAP) gene is deleted in over 47% of pancreatic cancers [44] and this deletion effectively removes a downstream metabolite (2-keto-4-methyl-thiobutyrate, MTOB), which is an inhibitor of ODC activity (**Figure 1**) [44]. MTAP and MTOB are important because ODC activity is known to promote tumor formation [37, 45]. We hypothesized that because MTAP and the p16 tumor suppressor gene are in such close proximity at 9p21, deletion in this region can create dual loss of both p16 and MTAP, which may promote tumor progression by removing a tumor suppressor gene and the ODC inhibitor, MTOB [44].

Cav-1

Polyamines have been shown to enter human cells via a caveolin-dependent mechanism (**Figure 1**), where low caveolin-1 (Cav-1) expression correlated with increased polyamine transport activity [34]. Interestingly, caveolin-1 expression becomes virtually undetectable in many metastatic cancer cells, which should increase their polyamine transport activity [46]. There are, however, conflicting reports in the literature regarding caveolin-1 levels in pancreatic cancers [46, 47] and a definitive study was needed to address this knowledge gap by defining the relationship between caveolin-1 expression and polyamine transport in pancreatic cancers because non-caveolin dependent pathways are also possible [31].

We note that recent studies further support the negative regulation of the PTS by Cav-1 in other tissues. Indeed, recent Cav-1 knockout (Cav-1 KO) experiments in vascular smooth muscle cells (VSMCs) demonstrated that the Cav-1 KO VSMCs had increased polyamine uptake relative to wild-type (wt) cells and that the Cav-1 KO cells were hyper-proliferative in the presence, but not the absence of exogenous polyamines [48]. In summary, Cav-1 was shown to negatively regulate polyamine uptake in VSMCs and the proliferative advantage of Cav-1 KO cells was critically dependent upon polyamine uptake [48, 49].

c-Myc

c-Myc was chosen due to the previously described correlations between Myc expression and polyamine metabolism [1, 36]. The potential of c-Myc to modulate *both* polyamine biosynthesis and transport in pancreatic cancers was an intriguing hypothesis to pursue. A strong correlation between c-Myc protein expression and V_{max} of ^{3}H-Spd uptake was observed in the current study further validating our selection of this protein.

ATP13A3

The selection of ATP13A3 as a potential biomarker of polyamine transport was based upon our previous work on polyamine transport ligands. We developed a series of fluorescent polyamine probes and optimized their structure for import via the polyamine transport system (PTS) in mammalian cells [9, 50]. These novel probes ranged from having one-, two- or three-appended polyamine chains on an aryl platform and are shown in **Figure 2**. Interestingly the one- and two-arm designs were shown to be PTS ligands that could enter and kill cells via the PTS [51]. The three-arm motifs were shown to be efficient polyamine transport inhibitors (PTIs) [14]. In 2010, one of the synthetic probes (**1a** in **Figure 2**) was used in *C. elegans* to identify a novel P_5-type ATPase (CATP-5), which was

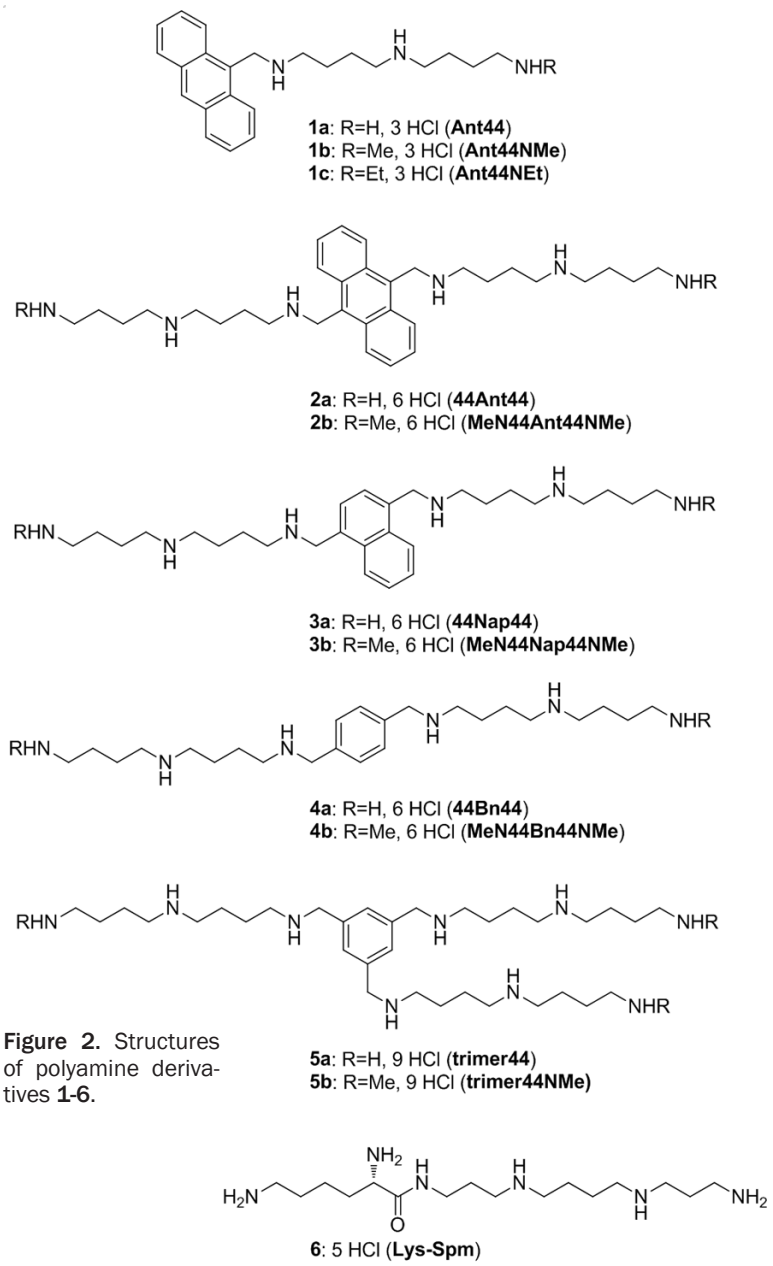

Figure 2. Structures of polyamine derivatives **1-6**.

shown to play a role in polyamine transport [52]. The human homologue of this worm gene is ATP13A3 and the findings with CATP-5 led us to investigate ATP13A3 as a potential marker for human polyamine transport.

Our study validated three putative biomarkers for polyamine transport (Cav-1, c-Myc and ATP13A3). In contrast, MTAP and p16 protein expression patterns did not correlate with V_{max} of ^{3}H-Spd import. We note that additional genes that could also be involved (e.g., ATP13A2 [53], glypican-1 [54-56], NOS-2, and SLC3A2) [31], were not part of this study.

PTI compounds

While compounds 1-4 in **Figure 2** were cytotoxic ligands for the PTS, compounds **5a**, **5b** and **6** were relatively non-toxic polyamine transport inhibitors (PTIs) [19, 57] and were compared in this study for their activity in combination with DFMO in human and murine pancreatic cancer cell lines. We note that all of these compounds have polyamines within their structure and were expected to be competitive inhibitors of polyamine transport.

Kinetic studies

The K_m for Spd and V_{max} experiments using radiolabeled Spd (^{3}H-Spd) were performed in the selected pancreatic cell lines as well as in two Chinese hamster ovary cell lines (CHO-K1 and CHO-MG cells). CHO-MG is a mutant of CHO-K1, which has no measurable polyamine uptake activity [33]. The CHO cell lines were included as controls to illustrate the effect in cell lines known to have high and low polyamine transport activity, respectively [14, 51, 58]. The results are shown in **Table 1**.

The experiments in **Table 1** identified L3.6pl as the cell line with the highest V_{max} and highest K_m. The L3.6pl cell line was isolated after six selection rounds for metastatic capacity using orthotopic transplantation [59]. Specifically, the L3.6pl cells had over three fold *higher polyamine uptake* (V_{max} = 24 nmol/mg protein/min) than the control HPNE cells (V_{max} = 1.8 nmol/mg protein/min) and utilized a transport system with more than *three-fold lower binding affinity*, as evidenced by the higher K_m value determined in this cell line (K_m = 0.67 μM in L3.6pl *vs* 0.19 μM for HPNE). We speculate that this low affinity pathway provides these cells with a scavenging pathway to harvest polyamine metabolites

Table 2. Cell line sensitivity to DFMO (72 h IC_{50}) and spermidine rescue challenge[a]

Cell line	72 h DFMO IC_{50} (mM)	% viability after 72 h incubation with Spd (1 μM) and the 72 h DFMO IC_{50} dose
HPNE	17 ± 0.6	60-62 (Very low)
L3.6pl	4.2 ± 0.11	89-93 (High)
Panc-1	3.8 ± 0.1	80-81 (Med)
Su 86.86	10.4 ± 0.44	80-85 (Med)
BxPC-3	14.4 ± 0.25	70-72 (Low)
AsPC-1	11.8 ± 0.44	50-60 (Not rescuable)
Capan-1	13.2 ± 0.5	26-43 (Not rescuable)
PanO2	0.5 ± 0.03	85-93 (High)
CHO-K1	4.2 ± 0.37	100-105 (High)
CHOMG	0.05 ± 0.005	50-55 (Not rescuable)

[a]'Spermidine Rescue Rank' as measured via the % viability observed when each cell line was incubated 72 h at 37°C in the presence of an IC_{50} dose of DFMO (listed above) and Spd (1 μM) was assigned as: High (≥ 90%), Medium (≥ 80-89%), Low (≥ 70-79%), Very low (> 60-69%) and not rescuable (≤ 60%). The rank is shown in parentheses (e.g., High, Med, Low).

from their surroundings resulting in a greater net import flux as seen in the V_{max} determinations.

The two CHO cell lines gave the expected striking differences in ^{3}H-Spd uptake. CHO-K1 cells had a K_m = 0.24 μM and V_{max} of 3 nmol/mg protein/min, while the CHO-MG line showed no measurable uptake (V_{max} = 0 nmol/mg protein/min) confirming its deficient uptake pathway.

We next determined the sensitivity of these cells to DFMO and the ability of exogenous Spd (1 μM) to rescue cells when treated at their IC_{50} dose of DFMO (**Table 2**). We assigned a 'spermidine rescue rank' based upon the ability of Spd (at 1 μM) to rescue these cells past certain viability thresholds. The data in **Table 2** were then compared to the V_{max} of untreated cells in **Table 1**. We hypothesized that DFMO-treated cell lines with high basal polyamine transport activity would import Spd more readily and retain high cell viability due to the ability of cells to interconvert Spd to either Put or Spm as needed (See **Figure 1**) [1].

As shown in **Table 2**, the cell lines demonstrated varying sensitivity to DFMO and some could-not be rescued from DFMO action by exogenous Spd addition (AsPC-1, Capan-1, and CHO-MG). Interestingly, the L3.6pl cell line, which had the highest V_{max}, was one of the most sensitive human cell lines to DFMO (72 h IC_{50} = 4.2 mM). Panc-1 (human), PanO2 (murine) and CHO (hamster) cells also showed significant rescue with exogenous Spd and had lower DFMO IC_{50} values (< 4.2 mM). As expected, the CHO-MG line was very sensitive to DFMO and was not rescuable with exogenous Spd due to the lack of a functional PTS. In general, cell lines with low DFMO 72 h IC_{50} values could be significantly rescued to higher viability with Spd in the DFMO/Spd rescue experiment. The correlation between DFMO 72 h IC_{50} value and % viability in the DFMO+Spd rescue experiment was good (r^2 = 0.53) suggesting that the sensitivity of the cell line to DFMO alone was predictive of its rescue by Spd. Indeed, cells with DFMO IC_{50} values ≤ 4.2 mM were rescued to > 80% viability by exogenous Spd (1 μM).

Our interpretation is that the cell lines that rely on polyamine import more than polyamine biosynthesis would give a higher V_{max} value for ^{3}H Spd import, higher Spd rescue rank, and lower DFMO IC_{50} value (e.g., L3.6pl cells). In contrast, cells with a heavy reliance upon polyamine biosynthesis and lower commitment to polyamine transport should give a lower V_{max} values, lower-Spd rescue rank, and a higher DFMO IC_{50} value (e.g., AsPC-1).

We were interested in how the dual blockade of polyamine biosynthesis and polyamine transport via the DFMO+PTI combination therapy affected the viability of cell lines with different DFMO sensitivities and V_{max} values. Earlier work had identified three PTIs (**5a**, **5b** and **6**) and these were screened in the L3.6pl cell line for this property [14]. A Spd rescue assay (**Figure 3**) was employed to rank the potency of each PTI as an EC_{50} value. The PTI toxicity profile (IC_{50} and IC_{10} values) were also determined in the different cell lines.

EC_{50} studies

As shown in **Figure 3**, cells were treated with the 72 h IC_{50} DFMO dose, a rescuing dose of Spd (1 μM), and increasing concentrations of the PTI compound to determine the EC_{50} value. In an ideal case, where DFMO gave 50% viability and Spd gave 100% rescue, the EC_{50} value would be halfway between these two outcomes, i.e., the concentration of the PTI needed to give 75% viability. **Figure 3** provides an illustration with PTI **5a**. The EC_{50} dose of the PTI is the concentration of the PTI needed to attain

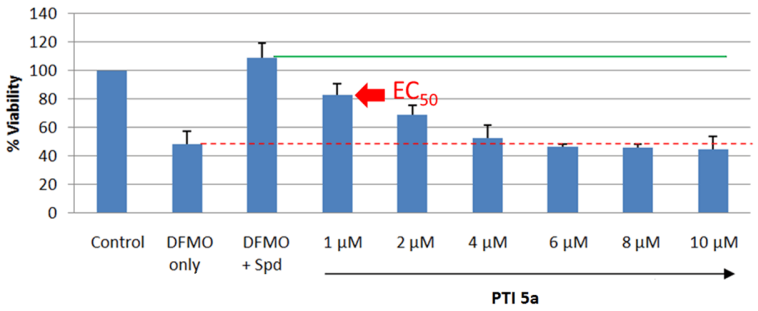

Figure 3. *Example 48 h EC_{50} determination experiment in L3.6pl cells*. The Control was set to 100% relative viability and was determined via the MTS reagent after 48 h growth period at 37°C. The DFMO-only cells were exposed to the 48 h DFMO IC_{50} dose (and gave the expected 50% viability); the DFMO+Spd cells were exposed to the 48 h IC_{50} DFMO dose and Spd (1 µM) (and shows increased viability due to Spd rescue); the remaining samples received a fixed DFMO IC_{50} dose, a fixed Spd rescuing dose (1 µM), and increasing concentrations of the PTI agent **5a**. As the PTI concentration is increased from 1 to 10 µM **5a**, less Spd enters the cells and lower relative viability is observed. The PTI **5a** was found to be non-toxic to L3.6pl cells at 2.5 µM during 48 h exposure. As seen in the graph above, the non-toxic PTI was able to block the rescuing effect of the added Spd. Note: PTI **5b** gave a similar result.The EC_{50} is shown graphically as the midpoint (in % viability) between the green and red lines, i.e. the DFMO+Spd and DFMO only controls.

Table 3A. PTI 72 h IC_{10} and IC_{50} values (in µM) across cell lines[a]

Cell Line	Trimer44 (**5a**) IC_{50} (IC_{10})	Trimer44NMe (**5b**) IC_{50} (IC_{10})	Lys-Spm (**6**) IC_{50} (IC_{10})
HPNE	17.2 ± 0.7 (4)	20.0 ± 0.1 (6)	> 200 (> 200)
L3.6pl	57.1 ± 3.3 (2.5)	75.0 ± 1.0 (5)	> 100 (> 100)
Panc-1	> 200 (20)	> 200 (20)	> 200 (>200)
Su86.86	39.2 ± 1.2 (4)	51.2 ± 1.3 (6)	> 200 (60)
BxPC-3	> 100 (50)	>100 (>100)	> 100 (> 100)
AsPC-1	> 100 (> 50)	>100 (>100)	> 100 (> 100)
Capan 1	ND	ND	ND
PanO2	46 ± 4.9 (8)	65.3 ± 5.6 (8)	> 200 (> 200)
CHOK1	> 100 (10)	> 100 (10)	> 100 (> 100)
CHOMG	66.9 ± 6.2 (10)	121.7 ± 3.9 (10)	> 100 (> 100)

[a]The IC_{50} and IC_{10} values represent the concentration of PTI needed to inhibit 50% and 10% of the relative cell viability, respectively after 72 h of incubation at 37°C. The IC_{10} value for these cells is the maximum amount of PTI compound that can be tolerated with minimal toxic effects to the cell (≤ 10% reduction in cell viability compared to untreated controls) after the 72 h incubation period. This represents the maximal PTI dose which would not bias assays by inducing significant toxic effects. Units are all in µM; ND = not determined.

the % viability halfway between the DFMO only and DFMO+Spd controls. The lower the EC_{50} value, the more potent the PTI is at blocking Spd import. Note: at the EC_{50} dose the PTI presumably blocks 50% of the entering Spd. Since reduced viability is the readout from this assay, it was critical that the PTI agent was not toxic at the concentrations tested. This was confirmed by separate control experiments via determination of the PTI IC_{10} value (i.e., the PTI concentration which gives 10% inhibition of cell viability). At the compound's IC_{10} value, the cells are ≥ 90% viable. Rewardingly, each PTI had EC_{50} values well below the respective PTI's IC_{10} value in each cell line.

The three PTI compounds (**5a**, **5b** and **6** [19]) all have polyamine motifs within their structure and were expected to be competitive inhibitors of polyamine transport. Indeed, Lys-Spm **6** has been established as a competitive inhibitor of Spd transport [19]. To demonstrate this with the tri-substituted motifs, we performed ^{3}H-Spd kinetic experiments with **5b** [14] and found that **5b** displayed competitive inhibition characteristics as expected (see Supporting information).

The three PTIs were then screened for their toxicity profiles (IC_{10} and IC_{50}) as well as for blockade of Spd import (EC_{50}) in several cell lines (see **Table 3A** and **3B**). Their respective K_i values are listed in the legend of **Table 1**. Understanding the cytotoxicity of these inhibitors via IC_{10} and IC_{50} measurements was critical because the EC_{50} assay relies upon a reduced viability endpoint which should not be derived from the intrinsic toxicity of the PTI compound itself, but from the ability of the PTI to out compete Spd for the putative extracellular receptor.

An ideal PTI should have a high 72 h IC_{50} value, a high 72 h IC_{10} value and a low 72 h EC_{50} value. Comparison between **Table 3A** (IC_{10}) and **3B** (EC_{50}) entries provides insight into the therapeutic window available for each PTI in each respective cell line. The Lys-Spm conjugate **6** gave low overall toxicity and good performance across multiple cell lines. The N-methyl derivative **5b** was consistently less toxic than **5a** as shown by its higher IC_{50} values in **Table 3A**. In contrast, **5a** was

Table 3B. PTI 72 h EC50 values (μM)

Cell Line	Trimer44 (**5a**) EC_{50}	Trimer44NMe (**5b**) EC_{50}	Lys-Spm (**6**) EC_{50}
HPNE	ND	ND	ND
L3.6pl	1.5 ± 0.1	3.2 ± 0.1	2.7 ± 0.2
Panc-1	2.9 ± 0.15	3.11 ± 0.18	2.06 ± 0.14
Su86.86	0.82 ± 0.03	1.96 ± 0.08	1.08 ± 0.01
BxPC-3	0.34 ± 0.02	1.03 ± 0.09	0.25 ± 0.02
AsPC-1	ND	ND	ND
Capan 1	ND	ND	ND
PanO2	0.61 ± 0.01	0.90 ± 0.07	6.00 ± 0.57
CHOK1	0.34 ± 0.02	0.90 ± 0.07	1.37 ± 0.05
CHOMG	ND	ND	ND

[a]All EC_{50} values were determined after 72 h incubation and represent the concentration of PTI (in μM) needed to provide a viability value halfway between the DFMO-only and the DFMO+Spd (1 μM) viability values. For example, when the DFMO-only control (added at its IC_{50} value) gave 50% viability and the DFMO+Spd control gave 100% viability, the EC_{50} value is the concentration of PTI needed to attain 75% viability in the presence of the IC_{50} dose of DFMO and the rescuing dose of Spd (1 μM) (Note: see **Figure 3** for an illustration). Importantly, all EC_{50} values were well below the IC_{10} values noted in **Table 3A**.

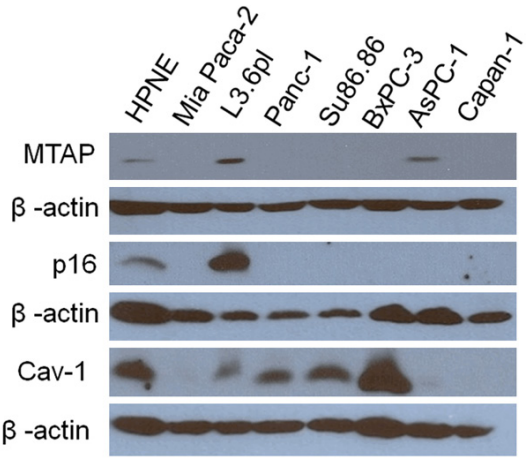

Figure 4. MTAP, p16, and caveolin-1 (Cav-1) protein expression versus β-actin expression in each cell line. MTAP expression was only detected in HPNE, L3.6pl, and AsPC-1 cell lines. HPNE and L3.6pl were p16 positive. MiaPaca-2 cells were included as a negative control.

more potent than **5b** as shown by its uniformly lower EC_{50} values (**Table 3B**). All three PTIs (**5a**, **5b**, and **6**) were individually effective in blocking Spd import in each of the rescuable cell lines at ≤ 6.5 μM. For most of the cell lines tested, the three PTIs had similar potencies. An exception was found in the PanO2 murine cell line, where **5a** was nearly ten-fold more potent than Lys-Spm **6**.

We noted that the human pancreatic cancer cell lines with the highest EC_{50} values (L3.6pl and Panc-1) also had the highest V_{max} values in **Table 1**. This suggested that cells with high basal polyamine uptake rates require more PTI to block their Spd import in the presence of DFMO. We speculated that this could be due to DFMO-induced increased expression of cell surface receptors associated with the PTS or activation of adifferent PTS.

The AsPC-1 and Capan-1 lines, were not studied in the EC_{50} assay as they were not rescuable with exogenous Spd. Pancreatic cancers with low to no cellular polyamine import are not expected to show effects from PTI treatment.However, these two cell lines were very interesting in terms of their sensitivity to the native polyamines. Neither AsPC-1 nor Capan-1 cells could be rescued from their respective 72 h IC_{50} dose of DFMO, even with 10 μM Spd. Capan-1 was not rescued from the 72 h IC_{50} dose of DFMO with either Put or Spd (at 5 μM), but was partially rescued up to 87% viability by Spm (5 μM). In contrast, AsPC-1 cells were not rescued with any of three native polyamines even at 10 μM.

Protein expression

DFMO was recently found to be a potential chemopreventative for K-ras-driven pancreatic cancers. Rao et al. found that changes in ODC signaling occur at early stages of pancreatic precursor lesions and increases as the tumor progresses in K-ras activated p48 $^{Cre/+}$-LSL-K-ras$^{G12D/+}$ mice [60]. DFMO treatment reduced the progression of pancreatic intraepithelial neoplasms (PanINs) and their progression to pancreatic ductal adenocarcinoma (PDAC) [60]. Interestingly, although DFMO inhibited PDAC in the K-ras mice, some tumor outgrowth was still observed [60]. The authors suggested that exogenous polyamines from dietary sources may explain the observed tumor escape [60]. This speculation is consistent with our observations, that exogenous Spd rescues pancreatic cancer cells from a DFMO challenge via the PTS. However, as seen in our DFMO study of various pancreatic cell lines, not all cell lines

Table 4. Relative Protein expression of Cav-1, ATP13A3 and c-Myc in untreated human pancreatic cancer cell lines along with the respective V_{max} values for ^{3}H Spd import and relative Spd rescue index[a]

Cell line	Cav-1	ATP13A3	c-Myc	V_{max} of untreated cells	Spd rescue index
HPNE	98.8	13.45	1	1.8	Very low
L3.6pl	100	100	100	24	High
Panc-1	126.4	5.7	75.3	13	Med
SU86.86	118.3	9.5	30.2	7	Med
BxPC-3	358.5	26.9	18.1	9	Low
AspC-1	16.6	1.8	4.6	2.3	Not rescuable
Capan-1	3.3	0.0	9.0	0.8	Not rescuable

[a]The blots were quantified by Image J software (NIH) and normalized by dividing by the β-actin expression level for each cell line. Entries represent protein expression and expressed in relative %, with the L3.6pl cell expression levels set to 100%. To illustrate how the relative protein expression patterns relate to the polyamine transport properties of the cell lines, the V_{max} value for ^{3}H-Spd import (nmoles Spd/mg protein/min) and the Spd rescue index observed with DFMO-treated cells are listed again for comparisons.

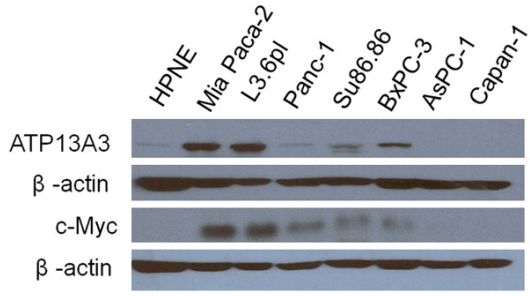

Figure 5. ATP13A3 and c-Myc protein expression versus β-actin expression in each cell line. ATP13A3 and c-Myc protein expression was barely detectable in the AsPC-1 and Capan-1 cell lines, which were not rescuable with Spd in previous DFMO experiments. MiaPaca-2 cells were included as a positive control for c-Myc and ATP13A3.

respond to exogenous Spd (e.g., AsPC-1) when exposed to an IC_{50} concentration of DFMO. The question remains: which proteins are responsible for this differential response?

There is significant evidence in the literature that DFMO can alter specific protein levels. For example, DFMO was shown to decrease Cav-1 mRNA expression in a dose-dependent manner and to increase the mRNA expression of the p21, p27 and p53 tumor suppressor genes [60]. Overexpression of Cav-1 in the pancreatic cancer cell line, Panc 10.05 that does not normally express Cav-1, induced an epithelial phenotype with increased expression of membranous E-cadherin and β-catenin [61]. Other studies have reported a decrease in c-Myc expression upon DFMO treatment [62-67]. Therefore, we looked at both the basal level of the target proteins and their relative changes upon DFMO treatment to better understand their roles in Spd rescue from DFMO. Western blots were used to determine relative protein expression in untreated and treated pancreatic cells lines.

No correlations between V_{max} and MTAP or p16 expression were observed (**Figure 4**) [5]. Cav-1 showed variable expression across these cell lines (**Table 4**). Based upon work by Gerner, Cav-1 is a negative regulator of polyamine transport and low caveolin-1 (Cav-1) expression should be associated with high polyamine import [6, 7]. In our study, Cav-1 alone was found to give inconsistent results as a predictor of V_{max}, consistent with the varied literature findings with this protein in pancreatic cancer [46, 47].

As shown in **Figure 5** and **Table 4**, basal c-Myc levels show a strong correlation ($r^2 = 0.90$) with V_{max} in untreated cells. This direct relationship was consistent with Bergeron's related experiments which showed increased polyamine uptake in Rat-1 cells upon N-myc transfection [36]. Thus, relative c-Myc expression correlates very well with basal polyamine transport activity. Basal c-Myc expression in untreated cells also had a good correlation ($r^2 = 0.86$) with K_m value. We were interested to see how c-Myc levels were modulated in the presence of DFMO. The level of c-Myc was shown to *decrease* upon DFMO treatment in L3.6pl cells (see Supporting information), contrary to what one might expect if c-Myc was involved in the Spd rescue process. We hypothesized that upon DFMO treatment the reduced c-Myc levels may trigger compensatory uptake pathways, possibly involving ATP13A3.

As shown in **Table 4**, basal ATP13A3 protein expression showed good correlation with V_{max} ($r^2 = 0.75$) and K_m ($r^2 = 0.82$). Cell lines with significant basal expression of ATP13A3 gave

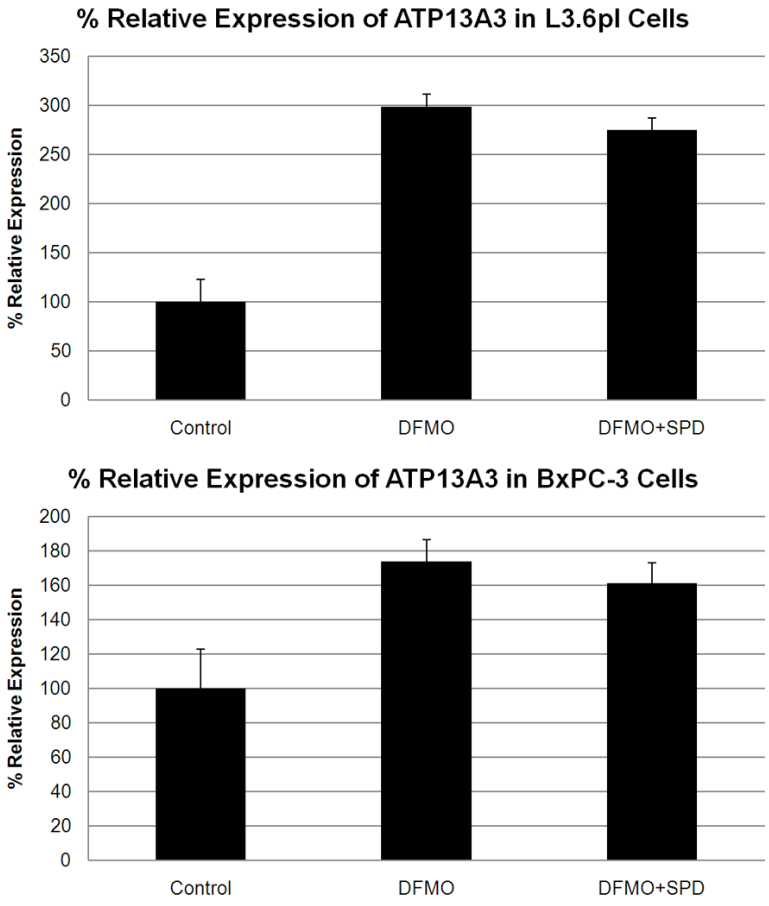

Figure 6. ATP13A3 protein levels in L3.6pl (top) and Bx-PC3 cells (bottom) in the presence of DFMO or DFMO+Spd as analyzed by Western blot. Expression was normalized using β-actin levels. Both cell lines showed a significant increase in relative ATP13A3 expression in the presence of the 48 h IC_{50} DFMO dose (8 mM) or DFMO + (1 μM Spd).

medium to high Spd rescue indices. Moreover, as shown in **Figure 6**, ATP13A3 was significantly *upregulated* (3 fold increase) in L3.6pl cells in the presence of DFMO alone or in combination with Spd (72 h incubation). This was also observed with BxPC-3 cells which showed a > 1.7 fold increase of ATP13A3 protein expression upon treatment with DFMO with or without Spd (**Figure 6**). Since ATP13A3 protein expression was increased in the presence of DFMO, we further investigated its role in DFMO-stimulated polyamine import using siRNA experiments.

siRNA experiments

siRNA experiments confirmed the role of ATP13A3 in Spd rescue of DFMO-treated L3.6pl cells. As shown in **Figure 7**, L3.6pl cells were treated for 48 h with either scrambled siRNA or ATP13A3 targeting siRNA (at 75 nM). Note: Parallel experiments confirmed the knockdown of ATP13A3 protein by Western blot (**Figure 7A**). The media was then removed, the cells were washed and fresh media added. A 48 h IC_{50} DFMO dose (8 mM) was then added along with Spd (1 μM). As expected, DFMO and the DFMO+Spd controls showed 50% and 90% viability, respectively. ATP13A3 siRNA caused a significant lower viability (62%) in the presence of DFMO+Spd. In contrast, the scrambled siRNA control showed the expected high viability (89%) in the presence of the same DFMO+Spd challenge.

Therefore, at first glance c-Myc and ATP13A3 showed strong correlations to polyamine transport activity, while Cav-1 did not. The mixed findings with Cav-1 could be explained, however, if one takes into account the relative ATP13A3 expression in cells. Indeed, low Cav-1 and high ATP13A3 expression may facilitate the cell's ability to escape DFMO therapy via caveolin-dependent endocytosis. This inverse relationship can be used to explain the rest of the results in **Table 4**. For example, Capan-1 cells, which had the lowest Cav-1 expression and were expected to have high polyamine transport activity, actually had the lowest V_{max} value and no detectable ATP13A3 to facilitate polyamine import via the putative DFMO-stimulated polyamine import process. A similar pattern was observed with AspC-1 cells.

We speculated that Cav-1 protein levels may also explain why BxPC-3 cells, which had the second highest ATP13A3 level measured, gave an unexpected low Spd rescue index. Indeed, as seen in **Table 4**, BxPC-3 had 3.6 fold higher Cav-1 levels than any other cell line tested in our study and these high Cav-1 levels did not

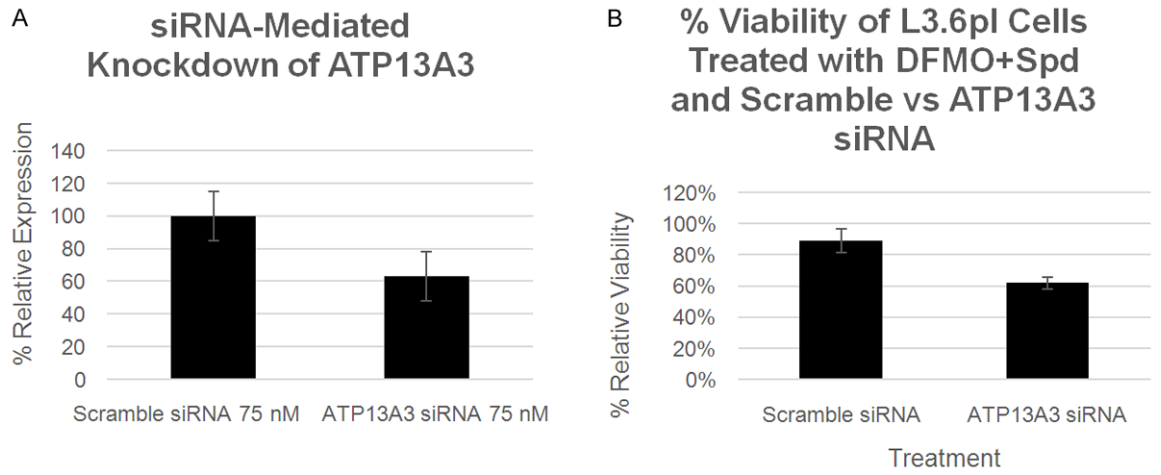

Figure 7. A: ATP13A3 protein levels in L3.6pl cells as analyzed by Western blot. Expression was normalized using β-actin protein levels. Decreased ATP13A3 expression was observed in the presence of the ATP13A3 siRNA versus the scrambled siRNA ($p < 0.05$). B: The effect of scrambled siRNA versus ATP13A3 siRNA on relative L3.6pl cell viability % when challenged with a 48 h IC_{50} DFMO dose (8 mM) and Spd (1 μM). Reduced ATP13A3 expression results in reduced rescue by Spd ($p < 0.01$). Other control experiments are shown in Figure S1 in the Supporting information.

significantly change in the presence of DFMO or DFMO+Spd (See Supporting information). This suggests that the high Cav-1 levels of BxPC-3 may limit its ability to scavenge polyamines via a caveolin-dependent process [68]. In contrast, L3.6pl cells had ~3.6-fold lower Cav-1 expression than BxPC-3, very high ATP13A3 expression and a high Spd rescue index.

Based upon these results, we propose that the relative ATP13A3 protein expression level provides an indicator of the cell's ability to escape DFMO, especially when viewed in the context of the cell's Cav-1 expression level. One interpretation of this apparent Cav-1 dependence is that cells with high ATP13A3 expression may escape DFMO using a caveolin-dependent polyamine uptake mechanism.

Biomarkers

The potential connection between basal expression of ATP13A3 and Cav-1 proteins was followed up using a bioinformatics approach to delineate the potential correlation between these two protein markers. We specifically focused on how the ATP13A3 and Cav-1 ratios vary in specific cancer types. Due to the lack of comprehensive protein expression profiles in the public databases for both markers, we looked at the available datasets for their relative mRNA levels.

First, we were interested to know whether the inverse expression pattern of ATP13A3 and Cav-1 existed in other human pancreatic cell lines. Analysis of mRNA expression profiles in the public domain, indeed, showed significant opposite expression patterns for ATP13A3 and Cav-1 in two independent pancreatic cell line collections; the general GSK-950 cell line set (27 pancreatic cell lines; **Figure 8A**), and the Sadandam-47 pancreas set (20 pancreatic cell lines; **Figure 8B**). This mRNA analysis provided supportive evidence that an inverse relationship does exist in specific human pancreatic cancer subtypes.

Next, we looked for similar inverse expression patterns in public human cancer patient samples. Our first analysis of public human sample data (Table S1) showed that both genes have good expression levels (500-1,000 after MAS-5.0 normalization). *ATP13A3* is almost always significantly expressed in human cancer samples, at stable, medium levels (99.6% of samples). *CAV1* is less widely expressed (76.8% of samples), and shows a higher variance in expression level. We found invariant, significant ATP13A3 over-expression in pancreas cancer versus normal tissue samples. However, we could not establish a robust inverse expression pattern with Cav-1, due to the paucity of public human pancreas cancer sets (Table S3).

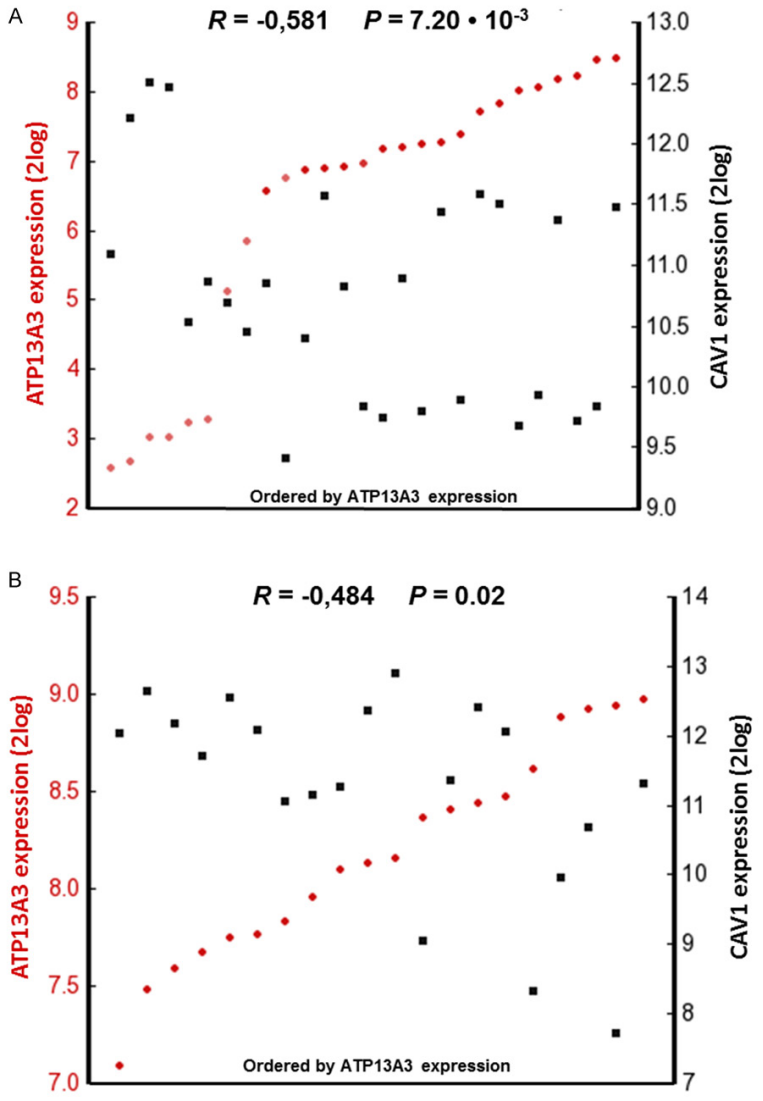

Figure 8. Inverse ATP13A3 versus CAV1 mRNA expression in two pancreatic cell line sets. Visual representation of *ATP13A3* and *CAV1* mRNA expression correlations calculated over (A) 27 pancreas cell lines in the GSK-950 dataset and (B) 20 pancreatic cancer cell lines in the Sadanandam-47 dataset as analyzed using R2. The tumors are ranked horizontally from left to right according to their *ATP13A3* mRNA expression as determined by Affymetrix array analyses (2log values). *ATP13A3* and *CAV1* expression values for each cell line are visualized with red circles and black rectangles, respectively. Dark and light colors denote samples with significant ("present call"), and absent expression, respectively. The correlations between *ATP13A3* and *CAV1* mRNA expression were inverse and statistically significant (calculated with a 2log Pearson test, see Materials and Methods).

We then widened our analysis to other cancer types for which more datasets were available. These include the most frequent and lethal human tumor types [69, 70]. The results show that ATP13A3 is often significantly overexpressed in tumor tissue in several different tumor sub-types. In these cancers, accompanying significantly lower Cav-1 tumor expression can be present (Tables S2 and S3). There was no evidence for ATP13A3 DNA copy gain versus Cav-1 copy loss (not shown). Remarkably, this high ATP13A3/low CAV1 tumor mRNA expression pattern appears to be specific for certain cancer types. With one exception (mantle cell lymphoma), it was not found in hematopoietic tumors. This inverse expression pattern was present much more often in solid tumor types and was especially frequent in epithelial tumors (carcinomas), more so thanin sarcomas and blastomas. **Figure 9A-D** shows examples for aggressive breast ductal carcinomas (high ATP13A3/low Cav-1) and rectal adenocarcinomas (low ATP13A3/high Cav-1). We also noted that several of the most common carcinomas, responsible for the large majority of the worldwide cancer deaths, like bladder, breast, cervix, colon, lung, ovary, and prostate cancer [69, 70] have high ATP13A3/low Cav-1 tumor expression. Finally, when we compared ATP13A3/Cav-1 expression in individual samples of datasets representing the carcinomas described above (and in Table S2), we found frequent, significant inverse correlations for *ATP13A3* versus *CAV1* expression for the whole dataset (Table S4). **Figure 9E** and **9F** show examples of these inverse correlations in large breast and colon datasets.

Together, these data suggest that inverse regulation of ATP13A3 and Cav-1 expression is present in aggressive, solid human cancers, and that high ATP13A3 versus low Cav-1 expression could be involved in tumor progression. These results provide for the first time *testable predictions* into which cancers will best respond to

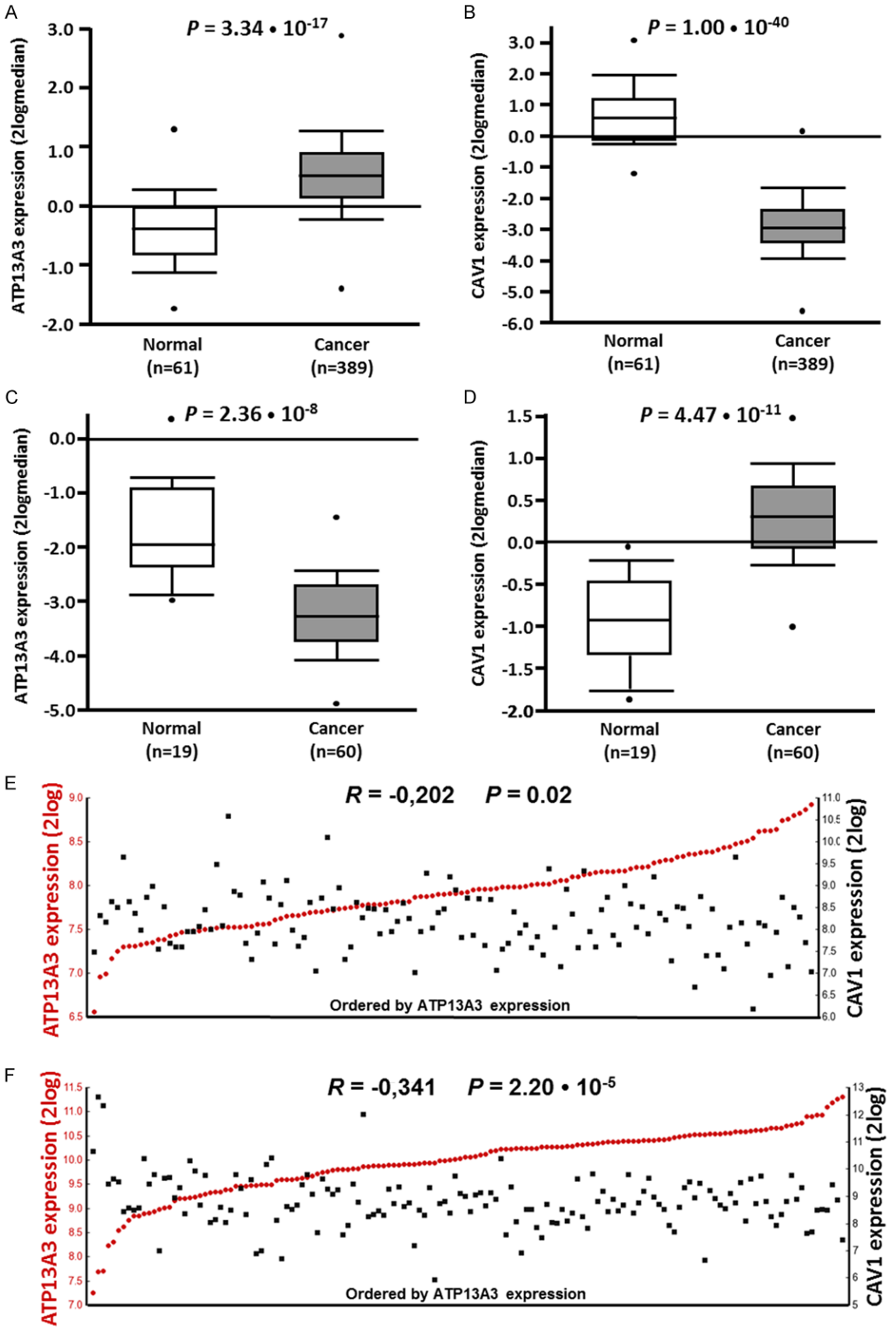
A
P = 3.34 • 10-17
ATP13A3 expression (2logmedian)
Normal (n=61)
Cancer (n=389)
B
P = 1.00 • 10-40
CAV1 expression (2logmedian)
Normal (n=61)
Cancer (n=389)
C
P = 2.36 • 10-8
ATP13A3 expression (2logmedian)
Normal (n=19)
Cancer (n=60)
D
P = 4.47 • 10-11
CAV1 expression (2logmedian)
Normal (n=19)
Cancer (n=60)
E
R = -0,202 P = 0.02
ATP13A3 expression (2log)
CAV1 expression (2log)
Ordered by ATP13A3 expression
F
R = -0,341 P = 2.20 • 10-5
ATP13A3 expression (2log)
CAV1 expression (2log)
Ordered by ATP13A3 expression

Figure 9. Significant ATP13A3 over- and Cav-1 under-expression and inverse correlations in other human cancer tissues. (A-D) Visual representation of ATP13A3 (A) and Cav-1 (B) mRNA expression in invasive ductal carcinoma samples in the TCGA-593 breast cancer dataset, and of ATP13A3 (C) and Cav-1 (D) mRNA expression in rectal adenocarcinoma samples in the TCGA-237 colon cancer dataset, as analyzed using Oncomine. Values are represented as 2log-median centered. *ATP13A3* and *CAV1* show mRNA over-and under-expression in tumor versus normal samples, respectively. The *P* values are calculated with a Student's t-test. More details can be found in Table S3 in the Supporting information. (E, F) Visual representation of ATP13A3 and Cav-1 mRNA expression correlations calculated over (E) all 123 samples of the Chin-123 breast cancer dataset or (F) all 148 samples of the Sugihara colon cancer dataset as analyzed using R2. The tumors are ranked horizontally from left to right according to their ATP13A3 mRNA expression as determined by Affymetrix array analyses (2log values). ATP13A3 and Cav-1 expression values for each tumor are visualized with red circles and black rectangles, respectively. The correlations between ATP13A3 and Cav-1 expression were inverse and highly significant (calculated with a 2log Pearson test, see Materials and Methods). More details can be found in Table S3.

DFMO. For example, cancers with low ATP13A3 and high Cav-1 (as seen with rectal adenocarcinomas) will likely respond to DFMO only, while other cancers with high ATP13A3 and low Cav-1 expression (as seen with invasive ductal carcinomas of the breast) may respond better to DFMO+PTI combination therapy.

Conclusions

Three PTIs (5a, 5b, and 6) were evaluated for their efficacy in treating pancreatic cancer cell lines in combination with DFMO. The results were rationalized in terms of the cells' relative commitment to polyamine biosynthesis and/or polyamine transport for growth. Cell lines with low V_{max} values, low Spd rescue rankings as well as low c-Myc and nearly undetectable ATP13A3 levels were considered to be heavily committed to polyamine biosynthesis and required high concentrations of DFMO to inhibit their growth (e.g., AsPC-1 and Capan-1). In contrast, cell lines with high V_{max}, high Spd rescue rankings, high relative c-Myc and ATP13A3 protein expression (e.g., L3.6pl) demonstrated significant commitment to polyamine transport and required lower DFMO concentrations to inhibit their growth. Interestingly, the human pancreatic cancer cell lines which were most sensitive to DFMO (i.e., gave the lowest DFMO IC_{50} values (Panc-1 and L3.6pl) also gave the highest EC_{50} values for the PTI agents indicating that more PTI was needed to competitively block the active polyamine transport systems of these cell lines. In addition, these cells had a Spd K_m that was significantly higher than the HPNE control (K_m = 0.19 μM) and 'non-rescuable' AsPC-1 and Capan-1 cell lines (K_m = 0.18 and 0.12 μM, respectively; **Table 2**) suggesting that a lower affinity PTS facilitates uptake of extracellular polyamines and may play a role in the ability of these cells to escape DFMO challenge.

Tumors which behave like AsPC-1 and Capan-1 cells should be sensitive to a DFMO-only therapy due to their significant commitment to polyamine biosynthesis but may require high doses of DFMO to affect their growth. In contrast, metastatic tumor cells like the L3.6pl cell line which demonstrate enhanced polyamine scavenging abilities should be more sensitive to the DFMO+PTI combination therapy (which blocks both polyamine biosynthesis and import). Most promising is that the combination therapy of DFMO+PTI should work with both tumor types, with the PTI showing low efficacy in tumors with poor transport activity, but high efficacy in tumors demonstrating high polyamine transport activity. In this regard, the PTI is an important adjuvant to DFMO.

Together the experiments in this study provide novel insights into the regulation of polyamine homeostasis in pancreatic cancers. The fact that the inverse relationship between high ATP13A3 and low Cav-1 mRNA expression exists in many specific human cancers is exciting and provides multiple opportunities for future experiments to test this hypothesis and to test these potential biomarker combinations and the DFMO+PTI combination therapy.

In summary, this paper demonstrates for the first time the role of ATP13A3 in polyamine transport in human pancreatic cancers and provides potential biomarkers to select tumors most susceptible to DFMO. This discovery provides a new approach to potentially stratify cancer patients in current and future clinical trials with DFMO [71, 72] and provides a potential 'catch-all' strategy in the form of a DFMO+PTI combination therapy for tumors which may escape.

Acknowledgements

The authors would like to thank Dr. Laurence von Kalm (UCF) for his helpful discussions

regarding this project, financial support by the 2011 Department of Defense Congressionally Directed Medical Research Program Peer Review Cancer Research Program (PRCRP) Discovery Award (#CA110724), Dr. Isaiah Fidler at the University of Texas M. D. Anderson Cancer Center for the generous gift of L3.6pl cells, Dr. Cheryl Baker at BioCurity Holdings, Inc. in Orlando, FL for the gift of hTERT-HPNE control cells and Dr. Wayne Flintoff at the University of Western Ontario, Canada for the gift of CHO-MG cells.

Disclosure of conflict of interest

None.

Address correspondence to: Otto Phanstiel IV, University of Central Florida College of Medicine, Department of Medical Education, 12722 Research Parkway, Orlando, Florida 32826, USA. E-mail: otto.phanstiel@ucf.edu

References

[1] Casero RA Jr and Marton LJ. Targeting polyamine metabolism and function in cancer and other hyperproliferative diseases. Nat Rev Drug Discov 2007; 6: 373-390.

[2] Igarashi K, Sakamoto I, Goto N, Kashiwagi K, Honma R and Hirose S. Interaction between polyamines and nucleic acids or phospholipids. Arch Biochem Biophys 1982; 219: 438-443.

[3] Gerner EW, Meyskens FL. Polyamines and cancer: old molecules, new understanding. Nat Rev Cancer 2004; 4: 781-792.

[4] Gerner EW. Cancer chemoprevention locks onto a new polyamine metabolic target. Cancer Prev Res (Phila) 2010; 3: 125-127.

[5] Soda K. The mechanisms by which polyamines accelerate tumor spread. J Exp Clin Cancer Res 2011; 30: 95-104.

[6] Meyskens FL Jr, Gerner EW. Development of Difluoromethylornithine (DFMO) as a chemoprevention agent. Clin Cancer Res 1999; 5: 945-951.

[7] Samal K, Zhao P, Kendzicky A, Yco LP, McClung H, Gerner E, Burns M, Bachmann AS and Sholler G. AMXT-1501, a novel polyamine transport inhibitor, synergizes with DFMO in inhibiting neuroblastoma cell proliferation by targeting both ornithine decarboxylase and polyamine transport. Int J Cancer 2013; 133: 1323-1333.

[8] Hsu PP and Sabatini DM. Cancer cell metabolism: Warburg and beyond. Cell 2008; 134: 703-707.

[9] Gardner RA, Delcros JG, Konate F, Breitbeil F, Martin B, Sigman M and Phanstiel O. *N*1-Substituent effects in the selective delivery of polyamine-conjugates into cells containing active polyamine transporters. J Med Chem 2004; 47: 6055-6069.

[10] Phanstiel O, Kaur N and Delcros JG. Structure-activity investigations of polyamine-anthracene conjugates and their uptake via the polyamine transporter. Amino Acids 2007; 33: 305-313.

[11] Muth A, Kamel J, Kaur N, Shicora AC, Ayene IS, Gilmour SK and Phanstiel O IV. Development of Polyamine Transport Ligands with Improved Metabolic Stability and Selectivity against Specific Human Cancers. J Med Chem 2013; 56: 5819-5828.

[12] Calvaresi EC and Hergenrother PJ. Glucose conjugation for the specific targeting and treatment of cancer. Chem Sci 2013; 4: 2319-2333.

[13] Phanstiel O and Archer JJ. Design of polyamine transport inhibitors as therapeutics. In: Casero, R.A. and Woster, P.M. , editors. Polyamine Drug Discovery. Royal Society of Chemistry; 2012. pp. 162-190.

[14] Muth A, Madan M, Archer JJ, Ocampo N, Rodriguez L and Phanstiel O IV. Polyamine transport inhibitors: design, synthesis, and combination therapies with difluoromethylornithine. J Med Chem 2014; 57: 348-363.

[15] Gerner EW, Meyskens FL Jr, Goldschmid S, Lance P, Pelot D. Rationale for, and design of, a clinical trial targeting polyamine metabolism for colon cancer chemoprevention. Amino Acids 2007; 33: 189-195.

[16] Svensson KJ, Welch JE, Kucharzewska P, Bengtson P, Bjurberg M, Pahlman S, Ten Dam GB, Persson L and Belting M. Hypoxia-mediated induction of the polyamine system provides opportunities for tumor growth inhibition by combined targeting of vascular endothelial growth factor and ornithine decarboxylase. Cancer Res 2008; 68: 9291-9301.

[17] Samal K, Zhao P, Kendzicky A, Yco LP, McClung H, Gerner E, Burns M, Bachmann AS and Sholler G. AMXT-1501, a novel polyamine transport inhibitor, synergizes with DFMO in inhibiting neuroblastoma cell proliferation by targeting both ornithine decarboxylase and polyamine transport. Int J Cancer 2013; 133: 1323-1333.

[18] Skorupski KA, O'Brien TG, Guerrero T, Rodriguez CO and Burns MR. Phase I/II clinical trial of 2-difluoromethyl-ornithine (DFMO) and a novel polyamine transport inhibitor (MQT 1426) for feline oral squamous cell carcinoma. Vet Comp Oncol 2011; 9: 275-282.

[19] Weeks RS, Vanderwerf SM, Carlson CL, Burns MR, O'Day CL, Cai F, Devens BH and Webb HK. Novel lysine-spermine conjugate inhibits polyamine transport and inhibits cell growth when

given with DFMO. Exp Cell Res 2000; 261: 293-302.
[20] Penchev VR, Rasheed ZA, Maitra A and Matsui W. Heterogeneity and targeting of pancreatic cancer stem cells. Clin Cancer Res 2012; 18: 4277-4284.
[21] Mohammed A, Janakiram NB, Madka V, Ritchie RL, Brewer M, Biddick L, Patlolla JM, Sadeghi M, Lightfoot S, Steele VE and Rao CV. Eflornithine (DFMO) prevents progression of pancreatic cancer by modulating ornithine decarboxylase signaling. Cancer Prev Res (Phila) 2014; 7: 1198-1209.
[22] Barrett T, Troup DB, Wilhite SE, Ledoux P, Rudnev D, Evangelista C, Kim IF, Soboleva A, Tomashevsky M, Marshall KA, Phillippy KH, Sherman PM, Muertter RN and Edgar R. NCBI GEO: archive for high-throughput functional genomic data. Nucleic Acids Res 2009; 37: D885-890.
[23] Revet I, Huizenga G, Chan A, Koster J, Volckmann R, van Sluis P, Ora I, Versteeg R and Geerts D. The MSX1 homeobox transcription factor is a downstream target of PHOX2B and activates the Delta-Notch pathway in neuroblastoma. Exp Cell Res 2008; 314: 707-719.
[24] Pegg AE. Regulation of ornithine decarboxylase. J Biol Chem 2006; 281: 14529-14532.
[25] Pegg AE. Mammalian polyamine metabolism and function. IUBMB Life 2009; 61: 880-894.
[26] Coffino P. Regulation of cellular polyamines by antizyme. Nat Rev Mol Cell Biol 2001; 2: 188-194.
[27] Zhu C, Lang DW and Coffino P. Antizyme2 is a negative regulator of ornithine decarboxylase and polyamine transport. J Biol Chem 1999; 274: 26425-26430.
[28] Mitchell JL, Leyser A, Holtorff MS, Bates JS, Frydman B, Valasinas AL, Reddy VK and Marton LJ. Antizyme induction by polyamine analogues as a factor of cell growth inhibition. Biochem J 2002; 366: 663-671.
[29] Mitchell JL, Simkus CL, Thane TK, Tokarz P, Bonar MM, Frydman B, Valasinas AL, Reddy VK and Marton LJ. Antizyme induction mediates feedback limitation of the incorporation of specific polyamine analogues in tissue culture. Biochem J 2004; 384: 271-279.
[30] Mitchell JL, Thane TK, Sequeira JM, Marton LJ and Thokala R. Antizyme and antizyme inhibitor activities influence cellular responses to polyamine analogs. Amino Acids 2007; 33: 291-297.
[31] Poulin R, Casero RA and Soulet D. Recent advances in the molecular biology of metazoan polyamine transport. Amino Acids 2012; 42: 711-723.
[32] Heston WD, Kadmon D, Covey DF and Fair WR. Differential effect of alpha-difluoromethylornithine on the in vivo uptake of 14C-labeled polyamines and methylglyoxal bis(guanylhydrazone) by a rat prostate-derived tumor. Cancer Res 1984; 44: 1034-1040.
[33] Eser S, Schnieke A, Schneider G and Saur D. Oncogenic KRAS signalling in pancreatic cancer. Br J Cancer 2014; 111: 817-822.
[34] Roy UK, Rial NS, Kachel KL and Gerner EW. Activated K-RAS increases polyamine uptake in human colon cancer cells through modulation of caveolar endocytosis. Mol Carcinogen 2008; 47: 538-553.
[35] Uemura T, Yerushalmi HF, Tsaprailis G, Stringer DE, Pastorian KE, Hawel L 3rd, Byus CV and Gerner EW. Identification and characterization of a diamine exporter in colon epithelial cells. J Biol Chem 2008; 283: 26428-26435.
[36] Chang BK, Libby PR, Bergeron RJ and Porter CW. Modulation of polyamine biosynthesis and transport by oncogene transfection. Biochem Biophys Res Commun 1988; 157: 264-270.
[37] Megosh L, Gilmour SK, Rosson D, Soler AP, Blessing M, Sawicki JA and O'Brien TG. Increased frequency of spontaneous skin tumors in transgenic mice which overexpress ornithine decarboxylase. Cancer Res 1995; 55: 4205-4209.
[38] Liu L, Rao JN, Zou T, Xiao L, Wang PY, Turner DJ, Gorospe M and Wang JY. Polyamines regulate c-Myc translation through Chk2-dependent HuR phosphorylation. Mol Biol Cell 2009; 20: 4885-4898.
[39] Weeks RS, Vanderwerf SM, Carlson CL, Burns MR, O'Day CL, Cai F, Devens BH and Webb HK. Novel lysine-spermine conjugate inhibits polyamine transport and inhibits cell growth when given with DFMO. Exp Cell Res 2000; 261: 293-302.
[40] Gysin S, Rickert P, Kastury K and McMahon M. Analysis of genomic DNA alterations and mRNA expression patterns in a panel of human pancreatic cancer cell lines. Genes Chromosomes Cancer 2005; 44: 37-51.
[41] Hamidi H, Lu M, Chau K, Anderson L, Fejzo M, Ginther C, Linnartz R, Zubel A, Slamon DJ and Finn RS. KRAS mutational subtype and copy number predict in vitro response of human pancreatic cancer cell lines to MEK inhibition. Br J Cancer 2014; 111: 1788-1801.
[42] Hayes CS, Burns MR and Gilmour SK. Polyamine blockade promotes antitumor immunity. Oncoimmunology 2014; 3: e27360.
[43] Bertino JR, Waud WR, Parker WB and Lubin M. Targeting tumors that lack methylthioadenosine phosphorylase (MTAP) activity: current strategies. Cancer Biol Ther 2011; 11: 627-632.
[44] Subhi AL, Tang B, Balsara BR, Altomare DA, Testa JR, Cooper HS, Hoffman JP, Meropol NJ

and Kruger WD. Loss of methylthioadenosine phosphorylase and elevated ornithine decarboxylase is common in pancreatic cancer. Clin Cancer Res 2004; 10: 7290-7296.

[45] Gilmour SK, Birchler M, Smith MK, Rayca K and Mostochuk J. Effect of elevated levels of ornithine decarboxylase on cell cycle progression in skin. Cell Growth Differ 1999; 10: 739-748.

[46] Lin M, DiVito MM, Merajver SD, Boyanapalli M and van Golen KL. Regulation of pancreatic cancer cell migration and invasion by RhoC GTPase and caveolin-1. Mol Cancer 2005; 4: 21-34.

[47] Tanase CP, Dima S, Mihai M, Raducan E, Nicolescu MI, Albulescu L, Voiculescu B, Dumitrascu T, Cruceru LM, Leabu M, Popescu I and Hinescu ME. Caveolin-1 overexpression correlates with tumour progression markers in pancreatic ductal adenocarcinoma. J Mol Histol 2009; 40: 23-29.

[48] Grossi M, Rippe C, Sathanoori R, Sward K, Forte A, Erlinge D, Persson L, Hellstrand P and Nilsson BO. Vascular smooth muscle cell proliferation depends on caveolin-1-regulated polyamine uptake. Biosci Rep 2014; 34: 729-740.

[49] Grossi M, Phanstiel O, Rippe C, Sward K, Alajbegovic A, Albinsson S, Forte A, Persson L, Hellstrand P and Nilsson BO. Inhibition of polyamine uptake potentiates the anti-proliferative effect of polyamine synthesis inhibition and preserves the contractile phenotype of vascular smooth muscle cells. J Cell Physiol 2016; 231: 1334-1342.

[50] Phanstiel O IV, Kaur N and Delcros JG. Structure-activity investigations of polyamine-anthracene conjugates and their uptake via the polyamine transporter. Amino Acids 2007; 33: 305-313.

[51] Muth A, Kamel J, Kaur N, Shicora AC, Ayene IS, Gilmour SK, Phanstiel O 4th. Development of polyamine transport ligands with improved metabolic stability and selectivity against specific human cancers. J Med Chem 2013; 56: 5819-5828.

[52] Heinick A, Urban K, Roth S, Spies D, Nunes F, Phanstiel O 4th, Liebau E and Luersen K. Caenorhabditis elegans P5B-type ATPase CATP-5 operates in polyamine transport and is crucial for norspermidine-mediated suppression of RNA interference. FASEB J 2010; 24: 206-217.

[53] Pinto Fde T, Corradi GR, Hera DP and Adamo HP. CHO cells expressing the human P(5)-ATPase ATP13A2 are more sensitive to the toxic effects of herbicide paraquat. Neurochem Int 2012; 60: 243-248.

[54] Melo SA, Luecke LB, Kahlert C, Fernandez AF, Gammon ST, Kaye J, LeBleu VS, Mittendorf EA, Weitz J, Rahbari N, Reissfelder C, Pilarsky C, Fraga MF, Piwnica-Worms D and Kalluri R. Glypican-1 identifies cancer exosomes and detects early pancreatic cancer. Nature 2015; 523: 177-182.

[55] Diamandis EP and Plebani M. Glypican-1 as a highly sensitive and specific pancreatic cancer biomarker. Clin Chem Lab Med 2016; 54: e1-2.

[56] Belting M, Mani K, Jonsson M, Cheng F, Sandgren S, Jonsson S, Ding K, Delcros JG and Fransson LA. Glypican-1 is a vehicle for polyamine uptake in mammalian cells: a pivital role for nitrosothiol-derived nitric oxide. J Biol Chem 2003; 278: 47181-47189.

[57] Muth A, Madan M, Archer JJ, Ocampo N, Rodriguez L and Phanstiel O. Polyamine transport inhibitors: design, synthesis, and combination therapies with difluoromethylornithine. J Med Chem 2014; 57: 348-363.

[58] Mandel JL and Flintoff WF. Isolation of mutant mammalian cells altered in polyamine transport. J Cell Physiol 1978; 97: 335-344.

[59] Bruns CJ, Harbison MT, Kuniyasu H, Eue I and Fidler IJ. In vivo selection and characterization of metastatic variants from human pancreatic adenocarcinoma by using orthotopic implantation in nude mice. Neoplasia 1999; 1: 50-62.

[60] Mohammed A, Janakiram NB, Madka V, Ritchie RL, Brewer M, Biddick L, Patlolla JM, Sadeghi M, Lightfoot S, Steele VE and Rao CV. Eflornithine (DFMO) Prevents Progression of Pancreatic Cancer by Modulating Ornithine Decarboxylase Signaling. Cancer Prev Res (Phila) 2014; 7: 1198-1209.

[61] Salem AF, Bonuccelli G, Bevilacqua G, Arafat H, Pestell RG, Sotgia F and Lisanti MP. Caveolin-1 promotes pancreatic cancer cell differentiation and restores membranous E-cadherin via suppression of the epithelial-mesenchymal transition. Cell Cycle 2011; 10: 3692-3700.

[62] Celano P, Baylin SB and Casero RA Jr. Polyamines differentially modulate the transcription of growth-associated genes in human colon carcinoma cells. J Biol Chem 1989; 264: 8922-8927.

[63] Celano P, Berchtold CM, Giardiello FM and Casero RA Jr. Modulation of growth gene expression by selective alteration of polyamines in human colon carcinoma cells. Biochem Biophys Res Commun 1989; 165: 384-390.

[64] Klinken SP, Holmes KL, Morse HC 3rd and Thorgeirsson SS. Transcriptional and post-transcriptional regulation of c-myc, c-myb, and p53 during proliferation and differentiation of murine erythroleukemia cells treated with DFMO and DMSO. Exp Cell Res 1988; 178: 185-198.

[65] Tao L, Kramer PM, Wang W, Yang S, Lubet RA, Steele VE and Pereira MA. Altered expression of c-myc, p16 and p27 in rat colon tumors and

its reversal by short-term treatment with chemopreventive agents. Carcinogenesis 2002; 23: 1447-1454.
[66] Raul F. Revival of 2-(difluoromethyl)ornithine (DFMO), an inhibitor of polyamine biosynthesis, as a cancer chemopreventive agent. Biochem Soc Trans 2007; 35: 353-355.
[67] Liu L, Li L, Rao JN, Zou T, Zhang HM, Boneva D, Bernard MS and Wang JY. Polyamine-modulated expression of c-myc plays a critical role in stimulation of normal intestinal epithelial cell proliferation. Am J Physiol Cell Physiol 2005; 288: C89-99.
[68] Uemura T and Gerner EW. Polyamine transport systems in mammalian cells and tissues. Methods Mol Biol 2011; 720: 339-348.
[69] Jemal A, Bray F, Center MM, Ferlay J, Ward E and Forman D. Global cancer statistics. CA Cancer J Clin 2011; 61: 69-90.
[70] International WCRF. http://www.wcrf.org/cancer_statistics/world_cancer_statistics.php.
[71] Saulnier Sholler GL, Gerner EW, Bergendahl G, MacArthur RB, VanderWerff A, Ashikaga T, Bond JP, Ferguson W, Roberts W, Wada RK, Eslin D, Kraveka JM, Kaplan J, Mitchell D, Parikh NS, Neville K, Sender L, Higgins T, Kawakita M, Hiramatsu K, Moriya SS and Bachmann AS. A Phase I Trial of DFMO Targeting Polyamine Addiction in Patients with Relapsed/Refractory Neuroblastoma. PLoS One 2015; 10: e0127246.
[72] Laukaitis CM and Gerner EW. DFMO: targeted risk reduction therapy for colorectal neoplasia. Best Pract Res Clin Gastroenterol 2011; 25: 495-506.

Supporting information

Supporting information is available from the corresponding author (OP) and includes siRNA experiment controls, and overall expression of ATP13A3 and Cav-1 in human cancers, the ATP13A3 over- and Cav-1 under-expression mRNA pattern in common cancers, extensive data tables obtained from our analysis of human cancer databases showing the inverse correlations between ATP13A3 and Cav-1 and the complete ATP13A3-Cav1 mRNA expression correlation data used for **Figure 9**.

Table S1. ATP13A3 and CAV1 mRNA expression in human cancer datasets

Gene	Expression		Column 1 shows the average MAS5.0-normalized data for mRNA expression, with their SEM, calculated over 130 independent cancer datasets representing most different cancer types in R2 (17,363 samples in total). Column 2 shows the percentage of samples with a present call indicative of significant mRNA expression. For comparison: *GAPDH* and *ACTB* household mRNA expression in these datasets ranges between 5,000 and 10,000.
	Mean	Present call	
ATP13A3	478.1 (± 20.3)	99.6%	
CAV1	888.4 (± 83.7)	76.8%	

Table S1 shows the widespread, medium-level expression of both ATP13A3 and CAV1. Both genes are usually expressed in cancer cells. Affymetrix mRNA arrays have a built-in weighing algorithm for perfectly homologous vs. non-perfect mismatched probes for each gene to distinguish between significant ("present call") and absent/background ("absent call") expression. The above information allows the definition of significant expression for each sample. The inverse correlations we found are, therefore, not based on just a few signals, and are likely robust. For these mRNA arrays and this normalization procedure, expression values are almost linear and allow the following rule-of-thumb: 50-100: low expression. Visible with a very good antibody on Western blot; 250-2500: good expression. Levels for most genes, Visible with any reasonable antibody; > 2500: high expression. Usually reserved for household genes. While the mean expression of ATP13A3 mRNA expression is lower than CAV1 mRNA expression, the ATP13A3 expression is almost invariant, while that of CAV1 is more variable and is absent in almost 25% of samples. As shown below in Table S2, it is the inverse correlation that is most striking, not the actual expression levels.

Table S2. ATP13A3 over- and CAV1 under-expression mRNA pattern in common cancers[a]

Type	Subtype	SETS	High ATP13A3	Low CAV1
Adrenal Gland	Adenoma, cortex	1	1	1
Bladder	Carcinoma, urothelial infiltrating	3	2	2
Breast	Carcinoma, ductal	4	2	4
Breast	Carcinoma, ductal and lobular mixed	2	1	2
Breast	Carcinoma, ductal invasive	6	3	6
Breast	Carcinoma, invasive	3	2	3
Breast	Carcinoma, lobular invasive	1	1	1
Breast	Carcinoma, male	1	1	1
Cervix	Carcinoma, squamous cell (SCC)	3	3	3
Colon	Adenocarcinoma, cecum	2	2	2
Colon	Adenocarcinoma, mucinous	2	2	1
Colon	Adenocarcinoma, NOS	2	2	2
Colon	Adenocarcinoma, rectal	3	3	2
Colon	Adenocarcinoma, rectal mucinous	2	2	1
Colon	Adenocarcinoma, rectosigmoid	2	2	1
Colon	Carcinoma, colorectal	2	2	1
Colon	Carcinoma, NOS	1	1	1
Germ cell	Seminoma	2	2	1
Liver	Dysplasia, liver cell	1	1	1
Lung	Carcinoma, squamous cell (SCC)	6	6	5
Lung	Mesothelioma, pleural malignant	1	1	1
Lymphoma	Mantle cell	1	1	1
Ovary	Adenocarcinoma, clear cell	2	1	2
Ovary	Adenocarcinoma, endometrioid	2	2	2
Ovary	Adenocarcinoma, mucinous	2	2	2
Ovary	Adenocarcinoma, serous	4	2	4

Ovary	Carcinoma, NOS	1	1	1
Ovary	Carcinoma, serous surface papillary	1	1	1
Ovary	Cystadenocarcinoma, serous	1	1	1
Prostate	Adenocarcinoma	1	1	2
Prostate	Carcinoma, NOS	14	10	11
Prostate	Neoplasia, intraepithelial	1	1	1
Skin	Melanoma, cutaneous	1	1	1
Stomach	Cancer, NOS	2	2	1
Vulva	Neoplasia, intraepithelial	1	1	1

[a]Tumor types and subtypes are indicated in the first two columns. Column 3 shows the total amount of sets and column 4-5 show the number of datasets that have significant *ATP13A3* tumor mRNA over-expression and *CAV1* under-expression, respectively, per tumor subtype. Text is on a green background if ≥ 50% of the datasets for that tumor subtype showed the inverse *ATP13A/CAV1* expression pattern. Data from Oncomine, complete data in Supplemental Table.

Table S3. Complete ATP13A3 and CAV1 mRNA expression used for Table S2 and **Figure 9A-D**

Type	Subtype	ATP13A3		CAV1		Set (size)	N	N
		P	Fold	P	Fold		Tumor	Normal
Adrenal Gland	Adenoma, cortex	4.70E-02	1.111	3.00E-03	-1.214	Giordano 2 (65)	22	10
Adrenal Gland	Carcinoma, cortex			1.90E-02	2.894	Giordano (19)	9	3
Adrenal Gland	Carcinoma, cortex	5.00E-03	1.199	2.40E-02	1.129	Giordano 2 (65)	29	10
Bladder	Cancer, superficial			1.80E-02	-2.815	Blaveri 2 (93)	27	3
Bladder	Cancer, superficial			7.48E-05	-2.391	Dyrskjot 3 (60)	28	9
Bladder	Cancer, superficial			7.37E-12	-3.128	Lee (256)	126	68
Bladder	Cancer, superficial	9.00E-03	-1.731	1.74E-18	-10.666	Sanchez-Carbayo 2 (157)	28	48
Bladder	Carcinoma, urothelial infiltrating	3.10E-02	1.462			Dyrskjot 3 (60)	13	9
Bladder	Carcinoma, urothelial infiltrating			2.96E-05	-2.022	Lee (256)	62	68
Bladder	Carcinoma, urothelial infiltrating	6.00E-03	1.248	1.30E-21	-3.880	Sanchez-Carbayo 2 (157)	81	48
Brain	Astrocytoma	1.00E-02	2.090	4.70E-02	5.614	Rickman (51)	45	6
Brain	Astrocytoma	9.00E-03	1.524			Shai (42)	5	7
Brain	Astrocytoma, anaplastic	3.30E-02	1.672	4.10E-02	1.466	Sun (180)	19	23
Brain	Astrocytoma, pilocytic			2.50E-02	3.861	Gutmann (15)	8	3
Brain	Glioblastoma			4.25E-04	2.934	Bredel 2 (54)	27	4
Brain	Glioblastoma	8.00E-03	-1.728	3.66E-09	8.409	Lee (101)	22	3
Brain	Glioblastoma			3.05E-04	2.878	Liang (38)	30	2
Brain	Glioblastoma	2.84E-04	1.863	2.12E-08	3.810	Murat (84)	80	4
Brain	Glioblastoma	1.40E-05	2.117	4.67E-06	3.153	Shai (42)	27	7
Brain	Glioblastoma	1.64E-05	2.898	5.47E-19	3.714	Sun (180)	81	23
Brain	Glioblastoma	2.32E-05	2.055	1.79E-21	5.771	TCGA (557)	542	10
Brain	Glioblastoma, malignant glioma			3.40E-02	47.793	Pomeroy (85)	10	4
Brain	Oligoastrocytoma, anaplastic			1.20E-02	-1.562	Bredel 2 (54)	6	4
Brain	Oligoastrocytoma, anaplastic	2.80E-02	2.368			French (33)	4	6
Brain	Oligodendroglioma			2.50E-02	-1.437	Bredel 2 (54)	5	4
Brain	Oligodendroglioma	3.97E-04	1.871			Shai (42)	3	7
Brain	Oligodendroglioma, anaplastic	2.00E-03	1.788	6.00E-03	1.676	French (33)	23	6
Breast	Adenocarcinoma, intraductal cribriform			1.00E-03	-5.777	TCGA (593)	3	61
Breast	Carcinoma	no data	no data	8.39E-13	-4.565	Curtis (2,136)	14	144
Breast	Carcinoma, ductal	1.60E-02	1.158	5.00E-03	-9.284	Perou (65)	36	3
Breast	Carcinoma, ductal	2.19E-05	4.208	2.42E-09	-8.398	Richardson 2 (47)	40	7
Breast	Carcinoma, ductal			2.01E-06	-5.473	Sorlie (85)	65	4
Breast	Carcinoma, ductal			9.14E-27	-5.462	Sorlie 2 (167)	94	4
Breast	Carcinoma, ductal and lobular invasive	no data	no data	1.68E-48	-5.400	Curtis (2,136)	90	144
Breast	Carcinoma, ductal and lobular invasive			9.05E-05	-8.837	TCGA (593)	3	61
Breast	Carcinoma, ductal and lobular mixed	1.30E-02	1.521	8.31E-12	-4.730	TCGA (593)	7	61
Breast	Carcinoma, ductal in situ	no data	no data	5.57E-06	-3.550	Curtis (2,136)	10	144

Breast	Carcinoma, ductal in situ epithelia	2.77E-04	1.615	1.28E-05	-4.516	Ma 4 (66)	9	14
Breast	Carcinoma, ductal in situ stroma	4.00E-02	1.387			Ma 4 (66)	11	14
Breast	Carcinoma, ductal invasive	no data	no data	8.68E-91	-7.821	Curtis (2,136)	1556	144
Breast	Carcinoma, ductal invasive			3.60E-02	-1.574	Karnoub (22)	7	15
Breast	Carcinoma, ductal invasive	6.00E-03	1.793	8.00E-03	-3.683	Ma 4 (66)	9	14
Breast	Carcinoma, ductal invasive			1.20E-02	-2.054	Radvanyi (63)	31	9
Breast	Carcinoma, ductal invasive	3.34E-17	1.885	1.00E-40	-11.297	TCGA (593)	389	61
Breast	Carcinoma, ductal invasive	3.90E-02	1.722	2.10E-02	-5.086	Turashvili (30)	5	10
Breast	Carcinoma, ductal invasive			3.30E-02	-3.885	Zhao (64)	37	3
Breast	Carcinoma, invasive	no data	no data	1.17E-12	-4.065	Curtis (2,136)	21	144
Breast	Carcinoma, invasive			6.00E-03	-4.771	Gluck (158)	154	4
Breast	Carcinoma, invasive	1.12E-06	1.500	1.92E-35	-7.607	TCGA (593)	76	61
Breast	Carcinoma, invasive stroma	3.07E-07	2.405	2.62E-31	-31.695	Finak (59)	53	6
Breast	Carcinoma, lobular			1.80E-02	-3.568	Perou (65)	4	3
Breast	Carcinoma, lobular			7.00E-03	-12.424	Sorlie (85)	4	4
Breast	Carcinoma, lobular			3.00E-03	-6.906	Sorlie 2 (167)	7	4
Breast	Carcinoma, lobular invasive	no data	no data	2.23E-60	-4.900	Curtis (2,136)	148	144
Breast	Carcinoma, lobular invasive	5.90E-04	1.335	8.58E-20	-6.366	TCGA (593)	36	61
Breast	Carcinoma, male	3.75E-09	2.072	1.14E-04	-8.963	TCGA (593)	3	61
Breast	Carcinoma, medullary	no data	no data	6.01E-28	-4.592	Curtis (2,136)	32	144
Breast	Carcinoma, mixed invasive			3.30E-02	-1.721	Radvanyi (63)	3	9
Breast	Carcinoma, mucinous	no data	no data	3.94E-37	-4.257	Curtis (2,136)	46	144
Breast	Carcinoma, mucinous			7.32E-06	-5.711	TCGA (593)	4	61
Breast	Carcinoma, tubular	no data	no data	6.91E-45	-3.784	Curtis (2,136)	67	144
Breast	Fibroadenoma			5.10E-04	-14.128	Sorlie (85)	3	4
Breast	Fibroadenoma			4.72E-04	-12.864	Sorlie 2 (167)	3	4
Breast	Neoplasm, benign	no data	no data	2.89E-04	-2.730	Curtis (2,136)	3	144
Breast	Tumor, phyllodes	no data	no data	6.00E-03	-4.268	Curtis (2,136)	5	144
Cervix	Cancer	3.17E-10	3.643			Pyeon (84)	20	8
Cervix	Carcinoma, squamous cell (SCC)	1.41E-04	2.250	3.50E-07	-1.684	Biewenga (45)	40	5
Cervix	Carcinoma, squamous cell (SCC)	1.82E-10	3.145	1.00E-02	-1.526	Scotto 2 (66)	32	21
Cervix	Carcinoma, squamous cell (SCC)	4.82E-07	2.713	1.00E-02	-1.767	Zhai (41)	21	10
Cervix	Neoplasia, intraepithelial squamous high grade			4.50E-02	-1.420	Zhai (41)	7	10
Colon	Adenocarcinoma	5.01E-04	1.572	3.10E-02	-1.310	Kaiser (105)	41	5
Colon	Adenocarcinoma	no data	no data	1.17E-09	-14.481	Notterman (36)	18	18
Colon	Adenocarcinoma	3.01E-10	2.096	2.75E-07	-3.070	TCGA (237)	101	19
Colon	Adenocarcinoma, cecum	3.00E-03	1.354	4.00E-03	-1.574	Kaiser (105)	17	5
Colon	Adenocarcinoma, cecum	3.07E-10	2.146	1.56E-07	-3.005	TCGA (237)	22	19
Colon	Adenocarcinoma, mucinous	1.00E-02	1.270			Kaiser (105)	13	5
Colon	Adenocarcinoma, mucinous	2.87E-05	1.707	1.00E-03	-1.929	TCGA (237)	22	19
Colon	Adenocarcinoma, rectal	2.10E-02	1.292			Kaiser (105)	8	5
Colon	Adenocarcinoma, rectal	4.60E-02	1.100	5.00E-03	-1.472	Skrzypczak (105)	45	24
Colon	Adenocarcinoma, rectal	4.47E-11	2.208	2.36E-08	-3.322	TCGA (237)	60	19
Colon	Adenocarcinoma, rectal mucinous	7.21E-05	2.121			Kaiser (105)	4	5
Colon	Adenocarcinoma, rectal mucinous	1.44E-04	1.960	2.77E-04	-3.406	TCGA (237)	6	19
Colon	Adenocarcinoma, rectosigmoid	1.89E-04	1.613			Kaiser (105)	10	5
Colon	Adenocarcinoma, rectosigmoid	3.40E-02	2.192	1.57E-05	-2.346	TCGA (237)	3	19
Colon	Adenoma	6.07E-06	1.520			Sabates-Bellver (64)	25	5
Colon	Adenoma	2.00E-02	1.180			Skrzypczak (105)	5	10
Colon	Adenoma			6.00E-03	-1.407	Skrzypczak 2 (40)	5	10
Colon	Adenoma, rectal	7.33E-04	1.925			Sabates-Bellver (64)	7	7
Colon	Carcinoma	1.96E-04	1.374	3.60E-02	-1.252	Skrzypczak (105)	5	10
Colon	Carcinoma, colorectal	2.84E-07	1.828	2.00E-03	-1.412	Hong (82)	70	12
Colon	Carcinoma, colorectal	1.00E-03	1.242			Skrzypczak (105)	36	24
Colon	Carcinoma, epithelia	3.91E-07	1.692			Skrzypczak (105)	5	10
Colon	Carcinoma, epithelia			5.00E-03	-1.834	Skrzypczak 2 (40)	5	10

Esophagus	Adenocarcinoma	4.00E-03	1.759	5.00E-03	5.799	Hao (48)	5	14
Esophagus	Adenocarcinoma			7.62E-04	1.323	Kim (118)	75	28
Esophagus	Adenocarcinoma	4.00E-03	1.689			Kimchi (24)	8	8
Esophagus	Barrett's			3.26E-05	2.233	Hao (48)	14	14
Esophagus	Barrett's	1.10E-02	-2.139			Kimchi (24)	8	8
Esophagus	Carcinoma, squamous cell (SCC)	4.14E-08	1.923			Hu (34)	17	17
Esophagus	Carcinoma, squamous cell (SCC)	2.84E-15	1.635	7.00E-03	1.389	Su 2 (106)	53	53
Germ cell	Carcinoma, embryonal	7.43E-07	2.304	7.10E-09	2.670	Korkola (107)	15	6
Germ cell	Carcinoma, embryonal			3.70E-02	1.962	Skotheim (30)	5	3
Germ cell	Mixed	2.82E-10	1.858	1.48E-05	1.777	Korkola (107)	41	6
Germ cell	Seminoma	1.00E-03	1.428			Korkola (107)	12	6
Germ cell	Seminoma	3.80E-02	1.237	8.70E-06	-2.742	Sperger Others (74)	23	14
Germ cell	Teratoma	2.90E-05	1.758	3.08E-10	4.376	Korkola (107)	14	6
Germ cell	Tumor, yolk sac	1.10E-06	3.492			Korkola (107)	9	6
Germ cell	Tumor, yolk sac	4.60E-02	1.341			Skotheim (30)	4	3
Head & Neck	Adenoma, parathyroid gland	8.00E-03	1.278	2.40E-02	1.438	Morrison (61)	35	5
Head & Neck	Adenoma, thyroid gland follicular			9.77E-04	-1.406	Giordano (99)	10	4
Head & Neck	Adenoma, thyroid gland oncocytic	8.68E-04	-1.228	1.63E-05	-1.443	Giordano (99)	7	4
Head & Neck	Carcinoma, floor of the mouth	4.79E-04	2.389	2.20E-02	3.723	Pyeon (84)	5	9
Head & Neck	Carcinoma, nasopharyngeal			1.90E-07	2.724	Sengupta (41)	31	10
Head & Neck	Carcinoma, oral cavity	4.00E-03	3.263	5.00E-03	3.366	Pyeon (84)	4	9
Head & Neck	Carcinoma, oropharyngeal	2.20E-04	2.412	5.00E-03	2.464	Pyeon (84)	6	9
Head & Neck	Carcinoma, salivary gland adenoid cystic	6.55E-04	1.853	2.10E-02	1.609	FriersonHF (22)	16	6
Head & Neck	Carcinoma, squamous cell (SCC)	4.00E-03	2.676	1.00E-03	2.650	Cromer (38)	34	4
Head & Neck	Carcinoma, squamous cell (SCC)	3.25E-10	3.355	1.40E-02	1.556	Ginos (54)	41	13
Head & Neck	Carcinoma, squamous cell (SCC) hypopha-ryngeal			3.20E-02	4.918	Schlingemann (12)	4	3
Head & Neck	Carcinoma, squamous cell (SCC) oral cavity	1.24E-11	2.571	1.41E-10	1.889	Peng (79)	57	22
Head & Neck	Carcinoma, squamous cell (SCC) tongue	2.45E-10	3.290	4.05E-05	2.203	Estilo (58)	31	26
Head & Neck	Carcinoma, squamous cell (SCC) tongue	2.34E-10	1.988	1.09E-04	2.170	Talbot Lung (93)	31	26
Head & Neck	Carcinoma, squamous cell (SCC) tongue	6.92E-04	1.766	1.30E-02	1.991	Ye (38)	26	12
Head & Neck	Carcinoma, thyroid gland anaplastic	6.00E-03	-1.160			Giordano (99)	4	4
Head & Neck	Carcinoma, thyroid gland follicular			2.74E-05	-1.392	Giordano (99)	13	4
Head & Neck	Carcinoma, thyroid gland follicular oncocytic	9.19E-04	-1.255	2.43E-05	-1.573	Giordano (99)	8	4
Head & Neck	Carcinoma, thyroid gland papillary			6.00E-03	-1.270	Giordano (99)	26	4
Head & Neck	Carcinoma, thyroid gland papillary	2.30E-02	-1.633	3.00E-02	-1.830	He (18)	9	9
Head & Neck	Carcinoma, thyroid gland papillary	2.70E-02	-1.504			Vasko (18)	14	4
Head & Neck	Carcinoma, thyroid gland papillary follicular variant			3.49E-06	-1.434	Giordano (99)	15	6
Head & Neck	Carcinoma, thyroid gland papillary tall cell variant			6.00E-03	-1.308	Giordano (99)	10	4
Head & Neck	Carcinoma, tongue	4.55E-07	2.295	3.91E-06	3.727	Pyeon (84)	15	4
Head & Neck	Hyperplasia, parathyroid	2.30E-02	1.322			Morrison (61)	8	5
Head & Neck	Neoplasia, non-familial multiple gland	9.00E-03	1.361			Morrison (61)	10	5
Kidney	Carcinoma, chromophobe cell			6.00E-03	4.516	Higgins (44)	3	2
Kidney	Carcinoma, chromophobe cell	4.00E-03	-1.634			Jones (92)	6	23
Kidney	Carcinoma, chromophobe cell	9.64E-04	-3.749	3.00E-03	4.721	Yusenko (67)	4	3
Kidney	Carcinoma, clear cell (ccRCC)	7.47E-05	1.983	2.09E-10	8.172	Gumz (20)	10	10
Kidney	Carcinoma, clear cell (ccRCC)			1.26E-04	5.272	Higgins (44)	26	2
Kidney	Carcinoma, clear cell (ccRCC)	4.17E-06	1.696	7.02E-21	9.349	Jones (92)	23	23
Kidney	Carcinoma, clear cell (ccRCC)			5.57E-07	9.378	Lenburg (18)	9	9
Kidney	Carcinoma, clear cell (ccRCC)	2.00E-03	2.715	8.04E-12	5.028	Yusenko (67)	26	3
Kidney	Carcinoma, clear cell (ccRCC) hereditary	1.09E-08	1.750	4.93E-11	7.077	Beroukhim (70)	32	10
Kidney	Carcinoma, clear cell (ccRCC) non-hereditary	2.00E-06	1.524	1.93E-13	8.387	Beroukhim (70)	27	10
Kidney	Carcinoma, papillary cell			3.40E-02	-2.309	Higgins (44)	4	2
Kidney	Carcinoma, papillary cell	1.22E-05	1.849	1.00E-02	1.860	Jones (92)	11	23
Kidney	Carcinoma, papillary cell	2.40E-02	2.642	7.00E-03	1.856	Yusenko (67)	19	3

Kidney	Oncocytoma	2.02E-08	-3.597	4.75E-05	1.838	Jones (92)	12	3
Kidney	Oncocytoma	2.00E-03	-2.800	2.76E-04	3.406	Yusenko (67)	4	3
Kidney	Wilms			5.54E-04	-2.195	Cutcliffe (35)	18	3
Leukemia	Hairy cell (HCL)			2.99E-04	5.626	Basso (336)	16	5
Leukemia	Leukemia/Lymphoma, T-cell acute adult			3.05E-06	9.872	Choi (47)	22	6
Leukemia	Leukemia/Lymphoma, T-cell chronic adult	6.21E-04	-1.652			Choi (47)	19	6
Leukemia	Lymphoblastic, B-Cell acute (B-ALL)	3.54E-12	-1.441			Haferlach (2,096)	147	74
Leukemia	Lymphoblastic, B-Cell acute (B-ALL)	2.86E-04	-1.360			Maia (28)	18	5
Leukemia	Lymphoblastic, B-Cell acute (B-ALL) pediatric	4.30E-02	1.659			Coustan-Smith (288)	238	4
Leukemia	Lymphoblastic, B-cell acute (B-ALL) pediatric	2.10E-11	-1.380	2.96E-05	1.130	Haferlach (2,096)	359	74
Leukemia	Lymphoblastic, pro-B acute (pro-B-ALL)	3.15E-10	-1.458	2.45E-08	-1.173	Haferlach (2,096)	70	74
Leukemia	Lymphoblastic, T-cell acute (T-ALL)			3.50E-02	-1.071	Haferlach (2,096)	174	74
Leukemia	Lymphoblastic, T-cell acute (T-ALL) pediatric	9.00E-03	2.411			Coustan-Smith (288)	46	4
Leukemia	Lymphocytic, chronic (CLL)	1.56E-05	-1.913			Basso (336)	34	5
Leukemia	Lymphocytic, chronic (CLL)	7.66E-15	-1.474	1.74E-06	1.122	Haferlach (2,096)	448	74
Leukemia	Myeloid, acute (AML)	4.10E-02	1.335	1.20E-02	1.930	Andersson (127)	23	6
Leukemia	Myeloid, acute (AML)	1.80E-02	-1.097	1.17E-14	1.352	Haferlach (2,096)	542	74
Leukemia	Syndrome, myelodysplastic (MDS)	3.00E-04	1.169	1.00E-03	1.094	Haferlach (2,096)	206	74
Liver	Carcinoma, hepatocellular (HCC)			3.00E-02	1.228	Chen (197)	104	76
Liver	Carcinoma, hepatocellular (HCC)	7.56E-06	-1.469	4.18E-06	1.829	Mas (115)	38	19
Liver	Carcinoma, hepatocellular (HCC)	2.80E-02	-1.167	1.00E-03	1.956	Roessler (43)	22	21
Liver	Carcinoma, hepatocellular (HCC)	1.60E-02	-1.081	9.06E-15	1.537	Roessler 2 (445)	225	220
Liver	Carcinoma, hepatocellular (HCC)	4.00E-03	-1.946			Wurmbach (75)	35	10
Liver	Cirrhosis	2.98E-07	-1.546	3.66E-12	3.050	Mas (115)	58	19
Liver	Cirrhosis	5.00E-03	-1.954	4.00E-03	1.941	Wurmbach (75)	13	10
Liver	Dysplasia, liver cell	1.60E-02	1.142	2.20E-02	-1.349	Wurmbach (75)	17	10
Lung	Adenocarcinoma			3.48E-17	-8.702	Beer (96)	86	10
Lung	Adenocarcinoma			7.63E-10	-18.950	Bhattacharjee (203)	132	17
Lung	Adenocarcinoma			9.31E-15	-7.455	Garber (73)	40	5
Lung	Adenocarcinoma	9.25E-07	1.680	2.38E-16	-5.163	Hou (156)	45	65
Lung	Adenocarcinoma			2.59E-46	-11.725	Selamat (116)	58	58
Lung	Adenocarcinoma			7.94E-08	-6.292	Stearman (39)	20	19
Lung	Adenocarcinoma			1.70E-12	-7.611	Su (66)	27	30
Lung	Adenocarcinoma	2.39E-04	1.200	2.17E-33	-6.393	Landi (107)	58	49
Lung	Adenocarcinoma	6.52E-05	1.354	2.69E-33	-4.377	Okayama (246)	226	20
Lung	Carcinoid	3.00E-03	-2.663	2.10E-13	-66.005	Bhattacharjee (203)	20	17
Lung	Carcinoma, large cell	9.60E-05	2.144	3.87E-11	-12.444	Hou (156)	19	65
Lung	Carcinoma, large cell	1.10E-02	2.486			Yamagata (31)	5	3
Lung	Carcinoma, small cell			3.19E-05	-41.875	Bhattacharjee (203)	6	17
Lung	Carcinoma, small cell			1.30E-02	-10.984	Garber (73)	4	5
Lung	Carcinoma, squamous cell (SCC)	5.00E-03	2.531	8.96E-06	-6.689	Bhattacharjee (203)	21	17
Lung	Carcinoma, squamous cell (SCC)	3.10E-02	1.377	2.26E-10	-8.268	Garber (73)	13	5
Lung	Carcinoma, squamous cell (SCC)	1.46E-08	2.130	1.09E-14	-1.711	Hou (156)	27	65
Lung	Carcinoma, squamous cell (SCC)	1.97E-09	1.941	8.00E-03	-1.711	Talbot (93)	34	26
Lung	Carcinoma, squamous cell (SCC)	3.80E-02	1.311	9.87E-06	-7.840	Wachi (10)	5	5
Lung	Carcinoma, squamous cell (SCC)	6.00E-03	2.230			Yamagata (31)	10	3
Lung	Mesothelioma, pleural malignant	9.00E-03	1.679	1.00E-03	-2.575	Gordon (54)	40	5
Lymphoma	Angioimmunoblastic, T-cell	1.86E-08	2.600	2.69E-05	6.141	Piccaluga (60)	6	5
Lymphoma	Burkitt's			7.08E-08	10.240	Basso (336)	17	5
Lymphoma	Burkitt's	4.07E-04	-1.392	2.70E-02	1.273	Brune (67)	5	5
Lymphoma	Centroblastic	4.80E-02	1.365	2.18E-14	14.838	Basso (336)	28	5
Lymphoma	Effusion, primary			2.00E-03	8.972	Basso (336)	9	5
Lymphoma	Follicular	3.90E-02	-1.727	7.69E-04	2.384	Basso (336)	6	5
Lymphoma	Follicular			8.00E-03	1.369	Brune (67)	5	5
Lymphoma	Follicular	7.00E-03	-1.297	5.37E-23	11.075	Compagno (136)	38	5
Lymphoma	Hodgkin's			2.45E-04	1.999	Brune (67)	12	5

Lymphoma	Hodgkin's, classical	2.10E-02	1.142	1.30E-02	1.326	Eckerle (64)	4	5
Lymphoma	Hodgkin's, nodular lymphocyte predominant	3.20E-02	1.136	1.00E-03	4.433	Brune (67)	5	5
Lymphoma	Large cell, anaplastic	3.91E-09	2.746	5.28E-05	6.090	Piccaluga (60)	6	5
Lymphoma	Large cell, anaplastic ALK-positive	2.00E-03	1.121	5.30E-05	1.965	Eckerle (64)	5	5
Lymphoma	Large cell, primary cutaneous anaplastic	2.50E-02	-1.707			Eckerle (64)	7	5
Lymphoma	Large, B-cell T-cell/histiocyte-rich			3.31E-04	2.105	Brune (67)	4	5
Lymphoma	Lymphoma, diffuse large B-cell (DLBCL)	2.42E-04	1.960	4.61E-09	9.840	Basso (336)	32	5
Lymphoma	Lymphoma, diffuse large B-cell (DLBCL)	4.10E-02	1.230	6.83E-05	1.650	Brune (67)	11	5
Lymphoma	Lymphoma, diffuse large B-cell (DLBCL)	2.60E-02	1.198	5.16E-27	16.343	Compagno (136)	44	5
Lymphoma	Lymphoma, diffuse large B-cell (DLBCL)-like activated	7.63E-04	1.530	1.19E-15	13.262	Compagno (136)	17	5
Lymphoma	Lymphoma, diffuse large B-cell (DLBCL)-like germinal	2.60E-02	-1.630	1.20E-11	10.997	Compagno (136)	9	5
Lymphoma	Mantle cell	2.50E-02	1.636	5.00E-03	-3.053	Basso (336)	8	5
Lymphoma	Marginal zone, B-cell			5.00E-03	1.869	Storz (27)	5	3
Lymphoma	T-cell, unspecified peripheral	9.45E-09	2.107	5.07E-05	4.782	Piccaluga (60)	28	5
Myeloma	Gammopathy, monoclonal of undetermined significance			3.10E-02	-1.418	Agnelli 3 (158)	11	5
Myeloma	Gammopathy, monoclonal of undetermined significance	1.60E-04	1.419			Zhan 3 (78)	44	22
Myeloma	Leukemia, plasma cell	4.00E-03	1.570			Agnelli 3 (158)	9	5
Myeloma	Leukemia, plasma cell	3.10E-02	1.526			Zhan (131)	5	37
Myeloma	Multiple	8.04E-09	1.873	6.00E-03	1.689	Zhan (131)	74	37
Myeloma	Multiple	1.40E-02	1.185			Agnelli 3 (158)	133	5
Myeloma	Smoldering	2.58E-05	2.145	4.60E-02	1.786	Zhan 3 (78)	12	22
Ovary	Adenocarcinoma, clear cell	2.00E-03	1.140	2.20E-08	-1.884	Hendrix (103)	8	4
Ovary	Adenocarcinoma, clear cell			9.34E-04	-4.935	Lu (50)	12	4
Ovary	Adenocarcinoma, endometrioid	3.43E-04	1.165	2.05E-12	-1.725	Hendrix (103)	37	4
Ovary	Adenocarcinoma, endometrioid	1.90E-02	1.237	1.00E-03	-4.725	Lu (50)	9	5
Ovary	Adenocarcinoma, mucinous	4.00E-03	1.103	2.09E-07	-1.558	Hendrix (103)	13	4
Ovary	Adenocarcinoma, mucinous	1.60E-02	1.585	1.80E-02	-2.764	Lu (50)	9	5
Ovary	Adenocarcinoma, serous			3.94E-04	-6.790	Adib (16)	12	4
Ovary	Adenocarcinoma, serous	5.70E-05	1.230	2.15E-11	-1.704	Hendrix (103)	41	5
Ovary	Adenocarcinoma, serous	1.00E-03	1.388	1.00E-03	-4.970	Lu (50)	20	5
Ovary	Adenocarcinoma, serous			1.52E-29	-23.044	Yoshihara (53)	43	10
Ovary	Carcinoma	2.68E-05	1.362	3.91E-10	-7.582	Bonome (195)	185	10
Ovary	Carcinoma, serous surface papillary	5.97E-04	3.416	8.20E-06	-46.045	Welsh (32)	28	4
Ovary	Cystadenocarcinoma, serous	5.92E-07	1.693	2.72E-06	-3.555	TCGA (594)	586	8
Pancreas	Adenocarcinoma	4.00E-03	2.160			Logsdon (27)	27	5
Pancreas	Adenocarcinoma, ductal	1.40E-09	2.079	5.00E-03	1.668	Badea (78)	39	39
Pancreas	Adenocarcinoma, ductal			3.80E-02	-1.295	Buchholz (38)	11	5
Pancreas	Adenocarcinoma, ductal			1.50E-02	1.540	Ishikawa (49)	24	25
Pancreas	Carcinoma	1.70E-02	1.468			Pei (52)	36	16
Prostate	Adenocarcinoma	3.30E-02	1.164	7.07E-05	-2.456	Vanaja (40)	27	8
Prostate	Adenocarcinoma			7.05E-04	-1.581	Wallace (89)	69	20
Prostate	Carcinoma			1.36E-06	-2.909	Arredouani (21)	13	8
Prostate	Carcinoma	4.77E-04	1.246	4.79E-11	-2.548	Grasso (122)	59	28
Prostate	Carcinoma	5.00E-03	1.222			Holzbeierlein (54)	39	4
Prostate	Carcinoma			1.92E-27	-3.278	Lapointe (112)	62	41
Prostate	Carcinoma	1.20E-02	1.430			LaTulippe (35)	32	3
Prostate	Carcinoma	2.00E-03	1.164	1.75E-07	-2.273	Liu (57)	44	13
Prostate	Carcinoma	4.90E-02	1.411	4.00E-03	-1.838	Luo 2 (30)	15	15
Prostate	Carcinoma	2.10E-02	2.004			Magee (15)	8	4
Prostate	Carcinoma	5.00E-03	2.165	8.00E-03	-1.606	Singh (102)	52	50
Prostate	Carcinoma	1.00E-03	1.235	4.79E-12	-2.059	Taylor 3 (185)	131	29
Prostate	Carcinoma	1.40E-02	1.573	1.10E-02	-1.713	Tomlins (101)	59	28
Prostate	Carcinoma			1.00E-03	-2.199	Varambally (19)	7	6

Prostate	Carcinoma	7.88E-04	1.363	1.68E-06	-3.000	Welsh (34)	25	9
Prostate	Carcinoma			6.69E-06	-2.105	Yu (112)	65	23
Prostate	Hyperplasia, benign stroma	3.00E-03	-1.706			Tomlins (101)	6	5
Prostate	Neoplasia, intraepithelial	4.00E-03	1.928	5.90E-04	-1.925	Tomlins (101)	13	23
Skin	Carcinoma, basal cell	3.20E-02	3.928			Riker (87)	15	4
Skin	Carcinoma, squamous cell (SCC)	3.30E-02	2.705			Nindl (15)	5	6
Skin	Carcinoma, squamous cell (SCC)	1.90E-02	4.985			Riker (87)	11	4
Skin	Melanoma, cutaneous			1.20E-02	-1.900	Riker (87)	14	4
Skin	Melanoma, cutaneous	6.00E-03	3.290	2.30E-02	-1.455	Talantov (70)	45	7
Skin	Nevus, benign melanocytic	5.00E-03	3.353	1.80E-02	1.661	Talantov (70)	18	7
Soft tissue	Fibrosarcoma	8.71E-04	2.957			Detwiller (54)	7	1
Soft tissue	Histiocytoma, malignant fibrous	4.82E-06	2.953	6.00E-03	2.756	Detwiller (54)	9	1
Soft tissue	Leiomyosarcoma			9.56E-05	-2.018	Barretina (158)	26	9
Soft tissue	Leiomyosarcoma	4.84E-04	3.313	3.00E-03	2.749	Detwiller (54)	6	1
Soft tissue	Leiomyosarcoma			1.50E-02	-2.231	Quade Uterus (24)	4	4
Soft tissue	Liposarcoma, dedifferentiated			1.76E-11	-3.208	Barretina (158)	46	9
Soft tissue	Liposarcoma, dedifferentiated	1.70E-02	1.845			Detwiller (54)	4	1
Soft tissue	Liposarcoma, myxoid/round cell	4.65E-05	-2.016	1.11E-07	-2.657	Barretina (158)	20	9
Soft tissue	Liposarcoma, pleomorphic			3.45E-05	-2.184	Barretina (158)	23	9
Soft tissue	Liposarcoma, pleomorphic	2.11E-04	2.217	2.40E-02	3.029	Detwiller (54)	3	1
Soft tissue	Liposarcoma, round cell	3.90E-02	1.447			Detwiller (54)	4	1
Soft tissue	Myxofibrosarcoma			2.61E-07	-2.683	Barretina (158)	31	9
Soft tissue	Sarcoma, synovial	1.00E-03	2.768			Detwiller (54)	4	1
Stomach	Adenocarcinoma, diffuse	3.70E-02	1.132	1.48E-04	1.794	Chen (132)	13	28
Stomach	Adenocarcinoma, diffuse	4.60E-02	1.114			DErrico (69)	6	31
Stomach	Adenocarcinoma, intestinal type	3.00E-02	1.106	1.35E-06	1.416	Chen (132)	63	27
Stomach	Adenocarcinoma, intestinal type	3.57E-06	1.725	1.60E-02	1.432	DErrico (69)	26	31
Stomach	Adenocarcinoma, mixed			1.30E-02	1.351	Chen (132)	8	27
Stomach	Adenocarcinoma, mixed	7.02E-08	2.187			DErrico (69)	4	31
Stomach	Cancer	7.31E-04	1.257	5.51E-04	-1.461	Cui (160)	80	80
Stomach	Cancer	2.30E-02	1.500			Wang (27)	12	12
Stomach	Tumor, gastrointestinal stromal (GIST)			7.00E-03	-2.775	Cho (90)	20	19
Uterus	Leiomyoma, uterine corpus			1.70E-02	-1.146	Crabtree (77)	50	27
Uterus	Leiomyosarcoma, uterine corpus			1.00E-03	-8.555	Quade (24)	9	4
Vulva	Neoplasia, intraepithelial	2.41E-05	1.639	7.61E-06	-1.940	Santegoets (19)	9	10

Shown are all Oncomine tumor (sub)types with significant results. Subtypes that have significant *ATP13A3* tumor mRNA over-expression and *CAV1* under-expression, respectively are on a green background. Tumor type and subtype are listed in the first two columns. Columns 3-4 and 5-6 show *P* value and Fold increased/decreased mRNA expression in tumor over (matched) normal tissue, respectively. *P* and Fold values are as determined by a 2log-median centered t-test using Oncomine default settings. Column 7 shows name, type, and size. Columns 8-9 show amount of tumor samples, and normal tissue samples used in the t-test, respectively. Results in red type are used as the examples in **Figure 9A-D**.

Table S4. Complete ATP13A3-CAV1 mRNA expression correlation data used for **Figure 9E**, **9F**

Cancer Type	ATP-CAV		Dataset				
	R	P	Name	Size	Array	Study	PubMed
Breast	-0.202	2.00E-02	Chin	124	Affymetrix HG U133A	E-TABM-158	17157792
Breast	-0.179	4.40E-03	Miller	251	Affymetrix HG U133A	GSE3494	16141321
Breast	-0.193	8.00E-06	TCGA Breast	528	Agilent G4502	TCGA	23000897
Breast	-0.218	3.40E-03	Wessels	178	Illumina HumanWG-6 v3.0	GSE34138	23203637
Colon	-0.241	1.50E-06	Domany	390	Affymetrix HG U133A	GSE41258	19359472
Colon	-0.694	3.40E-04	Hong	22	Affymetrix HG U133P2	GSE4107	17317818
Colon	-0.251	7.80E-03	Matsuyama	111	Affymetrix HG U133P2	GSE18105	20162577
Colon	-0.451	9.40E-07	Medema	108	Affymetrix HG U133P2	GSE33114	22056143
Colon	-0.287	9.20E-04	Olschwang	130	Affymetrix HG U133P2	GSE37892	n.y.
Colon	-0.182	1.80E-03	Sieber	290	Affymetrix HG U133P2	GSE14333	19996206
Colon	-0.130	1.00E-02	SieberSmith	355	Affymetrix HG U133P2	*	22115830
Colon	-0.205	1.00E-02	Skrzypczak	145	Affymetrix HG U133P2	GSE20916	20957034
Colon	-0.341	2.20E-05	Sugihara	148	Affymetrix HG U133P2	GSE21510	21270110
Colon	-0.328	9.90E-06	TCGA Colon	174	Agilent G4502	TCGA	22810696
Colon	-0.296	2.00E-02	Uddin	59	Affymetrix HG U133P2	GSE23878	21281787
Liver	-0.225	4.10E-03	Cillo	161	Agilent-014850 HG 4x44K	GSE54236	25666192
Lung	-0.437	1.50E-05	Farez-Vidal	91	Affymetrix HG U133P2	GSE18842	20878980
Lung	-0.275	5.20E-04	Hou	156	Affymetrix HG U133P2	GSE19188	20421987
Lung	-0.495	1.60E-07	Muley	100	Affymetrix HG U133P2	GSE33532	n.y.
Lung	-0.176	3.60E-04	Plamadeala	410	Affymetrix HG U133P2	GSE63074	n.y.
Ovary	-0.100	2.00E-02	TCGA Ovary	541	Agilent G4502	TCGA	21720365
Ovary	-0.225	5.00E-02	Wong	77	Affymetrix HG U133P2	GSE40595	23824740
Prostate	-0.240	2.00E-02	Ambs	89	Affymetrix HG U133A	GSE6956	18245496

[a]Column 1 shows tumor type, columns 2-3 the *R* and *P* values of the 2log Pearson correlation tests for *ATP13A3* versus *CAV1* expression in R2. A negative R value indicates a negative correlation coefficient and a *P* value < 0.05 is considered statistically significant. Columns 4-8 contain dataset properties: R2 dataset name, amount of samples, array type, study number, and PubMed ID, respectively. GSE, TCGA, or E-TABM indicate NCBI GEO, TCGA, or EBI datasets, respectively n.y. means not yet published. *indicates GSE14333/17537/17538. Results in red type are used as the examples in **Figure 9E**, **9F**.

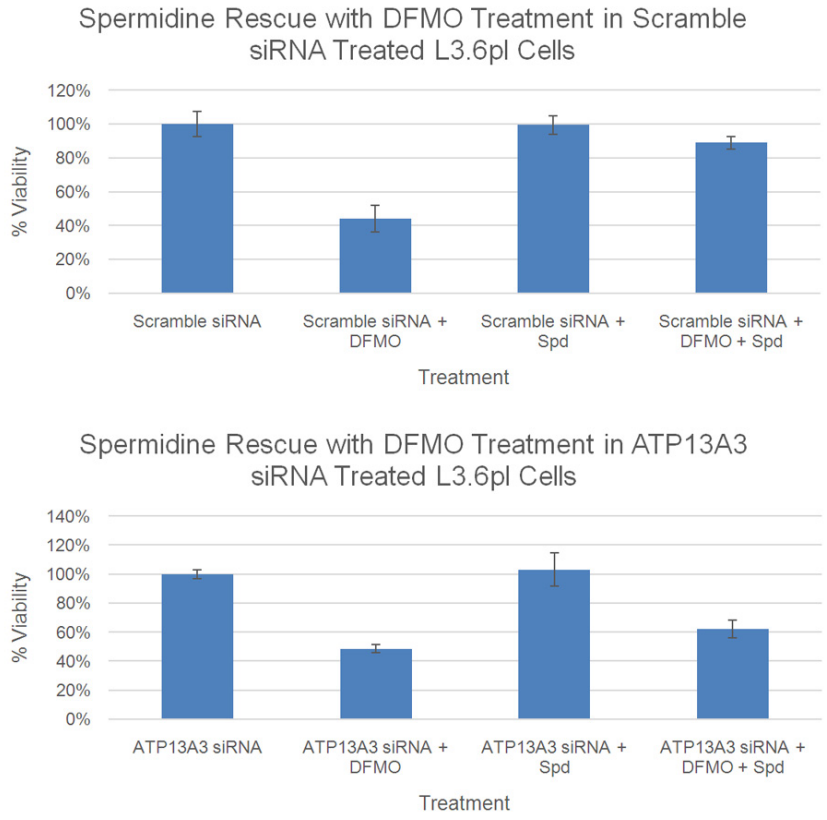

Figure S1. siRNA experiments in L3.6pl pancreatic cancer cells with scrambled vs ATP13A3 siRNA showing relative viability changes in the presence of the 48 h IC_{50} DFMO dose, spermidine (Spd, 1 μM) or the combination of DFMO+Spd. Comparison of the rightmost columns (in the top and bottom panels) are consistent with ATP13A3 protein playing a role in the spermidine rescue of DFMO-treated cells.

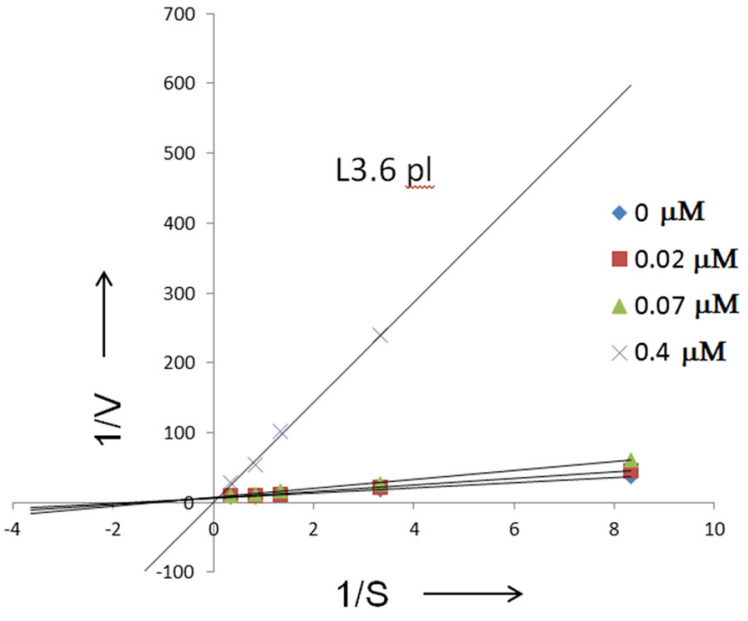

Figure S2. Competition experiments with PTI compound **5b** and ^{3}H-Spd. A classic competitive inhibitor kinetic profile (K_i of 5b = 55 nM) was obtained, where the x-intercept changes and the y-intercept remains constant.

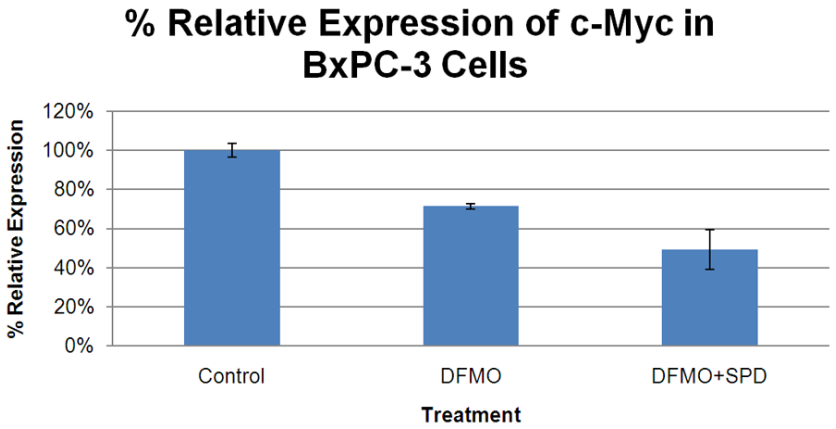

Figure S3. Decreased c-Myc protein expression observed in the presence of DFMO (72 h IC_{50} dose, 14.4 mM) or 72 h IC_{50} DFMO dose+Spd (1 μM) in BxPC-3 cells. Briefly, cells were grown in RPMI 1640 (Gibco), supplemented with 10% fetal bovine serum (Atlanta Biologicals) and penicillin/streptomycin (Gibco). After trypsinization, the cells were allowed 24 hours for reattachment before adding the appropriate drug or vehicle in PBS. DFMO was dosed at the respective IC_{50} values for each cell line, 14.4 mM (BxPC-3), and spermidine was dosed at 1 μM. The cells were incubated for 72 hours with 250 μM aminoguanidine present in the media. After 72 hours, the cells were collected and protein extracted in RIPA buffer for quantification via BCA assay and subsequent loading onto an SDS-PAGE gel. The primary antibody against c-Myc was rabbit monoclonal from Abcam, and against β-actin was mouse monoclonal from Sigma-Aldrich. The secondary antibodies used included goat anti-rabbit and goat anti-mouse (for β-actin) antibodies from Santa Cruz Biotechnology.

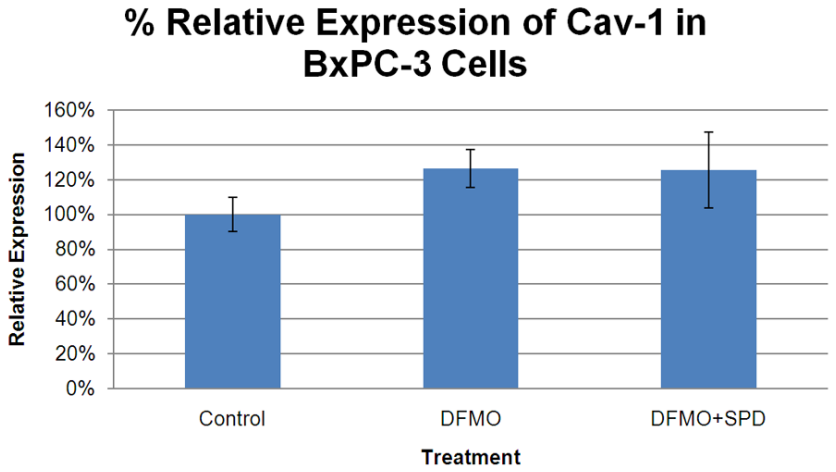

Figure S4. Relative expression of Cav-1 in the presence of the 72 h DFMO IC_{50} dose alone or in combination with Spd (1 μM) in BxPC-3 pancreatic cancer cells. The relatively high initial caveolin-1 levels in BxPC-3 cells did not decrease under these conditions and may explain why BxPC-3 cells were not highly rescuable by exogenous Spd, even though BxPC-3 cells had relatively high ATP13A3 expression.